© 2020. Published by The Company of Biologists Ltd | Biology Open (2020) 9, bio053421. doi:10.1242/bio.053421

RESEARCH ARTICLE

Vps54 regulates *Drosophila* neuromuscular junction development and interacts genetically with Rab7 to control composition of the postsynaptic density

Prajal H. Patel[1,*], Emily C. Wilkinson[1,*], Emily L. Starke[1], Malea R. McGimsey[1], J. Todd Blankenship[1,2] and Scott A. Barbee[1,2,‡]

ABSTRACT

Vps54 is a subunit of the Golgi-associated retrograde protein (GARP) complex, which is involved in tethering endosome-derived vesicles to the *trans*-Golgi network (TGN). In the wobbler mouse, a model for human motor neuron (MN) disease, reduction in the levels of Vps54 causes neurodegeneration. However, it is unclear how disruption of the GARP complex leads to MN dysfunction. To better understand the role of Vps54 in MNs, we have disrupted expression of the *Vps54* ortholog in *Drosophila* and examined the impact on the larval neuromuscular junction (NMJ). Surprisingly, we show that both null mutants and MN-specific knockdown of *Vps54* leads to NMJ overgrowth. Reduction of *Vps54* partially disrupts localization of the t-SNARE, Syntaxin-16, to the TGN but has no visible impact on endosomal pools. MN-specific knockdown of *Vps54* in MNs combined with overexpression of the small GTPases Rab5, Rab7, or Rab11 suppresses the *Vps54* NMJ phenotype. Conversely, knockdown of *Vps54* combined with overexpression of dominant negative Rab7 causes NMJ and behavioral abnormalities including a decrease in postsynaptic Dlg and GluRIIB levels without any effect on GluRIIA. Taken together, these data suggest that *Vps54* controls larval MN axon development and postsynaptic density composition through a mechanism that requires Rab7.

KEY WORDS: *Drosophila*, GARP, Rab7, Vps54, Neurodevelopment, Neuromuscular junction

INTRODUCTION

Endocytic trafficking is critical for many specialized processes in neurons including axon growth, guidance, plasticity, and for the maintenance of cellular homeostasis (Wojnacki and Galli, 2016). Disruption of endocytic trafficking pathways can cause neurodevelopmental defects and contribute directly to neurodegeneration (Schreij et al., 2016). A destabilizing point mutation in the gene encoding the vacuolar protein sorting-associated protein 54 (*Vps54*) is responsible for age-progressive motor neuron (MN) degeneration observed in the wobbler mouse model for human MN disease (Schmitt-John et al., 2005). *Vps54* loss-of-function in the mouse causes embryonic lethality and is characterized by the underdevelopment of MNs and cardiac muscle. Vps54 is a core subunit of the evolutionarily conserved Golgi-associated retrograde protein (GARP) complex, which localizes to the *trans*-Golgi network (TGN) and is involved in tethering retrograde transport carriers derived from endosomes (Bonifacino and Hierro, 2011). It has been postulated that the reduction of Vps54 levels, and thus a compensatory disruption of the GARP complex, contributes directly to MN degeneration (Moser et al., 2013; Schmitt-John, 2015).

GARP is a ubiquitously expressed complex composed of the Vps51, Vps52, Vps53 and Vps54 proteins (Conibear and Stevens, 2000). Within this complex, the Vps54 N-terminus binds to soluble *N*-ethylmaleimide-sensitive fusion protein attachment protein receptors (SNAREs). Vps54 interacts with SNAREs involved in retrograde transport including: Syntaxin-6 (Stx6), Syntaxin-16 (Stx16), and Vamp4 and is required for t-SNARE assembly (Pérez-Victoria and Bonifacino, 2009). In contrast, the C-terminal domain interacts with endosomes and is dispensable for both GARP and t-SNARE complex formation (Quenneville et al., 2006). Knockdown of Vps54 and other GARP subunits result in defects in retrograde transport of vesicles including those carrying the mannose-6-phosphate receptor (M6PR) and some v-SNAREs (Conibear and Stevens, 2000; Pérez-Victoria and Bonifacino, 2009; Pérez-Victoria et al., 2008; Quenneville et al., 2006). Disruption of GARP proteins also causes defects in the transport of some glycosylphosphatidylinositol (GPI)-anchored and transmembrane proteins derived from the TGN, suggesting that GARP may have an important function in anterograde membrane trafficking (Hirata et al., 2015). In addition to endosomal trafficking defects, knockdown of the GARP subunits in mammalian cells can cause lysosome dysfunction (Pérez-Victoria and Bonifacino, 2009; Pérez-Victoria et al., 2008). Together, these data suggest that Vps54 plays an important role in endolysosomal trafficking pathways in eukaryotes ranging from yeast to humans.

The glutamatergic *Drosophila melanogaster* larval neuromuscular junction (NMJ) is a well-characterized synapse that is used as a model system to study both neurodevelopmental and neurodegenerative processes (Deshpande and Rodal, 2016). In order to better understand the function of Vps54 in MNs, we have examined the development of the NMJ following depletion of the single *Drosophila* ortholog of *Vps54* (called '*scattered*' or '*scat*'). Here we show that both disruption of *scat* expression in an amorphic mutant and MN-specific reduction of expression via transgenic RNAi causes overgrowth of the larval NMJ. Unlike what is seen in yeast and mammalian cells, depletion of *scat* has no impact on the size, number, or localization of either early or late endosomes (EEs and LEs)

[1]Department of Biological Sciences, University of Denver, Denver, CO 80210, USA. [2]Molecular and Cellular Biophysics Program, University of Denver, Denver, CO 80210, USA.
*These authors contributed equally to this work

‡Author for correspondence (scott.barbee@du.edu)

S.A.B., 0000-0001-9349-9397

Received 4 May 2020; Accepted 22 July 2020

Biology Open (2020) 9, bio053421. doi:10.1242/bio.053421

(Palmisano et al., 2011; Quenneville et al., 2006). Both phenotypes are distinctly different from those reported in *Vps54* reduction-of-function (wobbler) and loss-of-function mouse models (Palmisano et al., 2011; Schmitt-John et al., 2005). The MN-specific knockdown of *scat* paired with overexpression of Rab5, Rab7 and Rab11, all suppress *scat* neurodevelopmental NMJ phenotypes. Conversely, presynaptic knockdown of *scat* combined with disruption of Rab7 function significantly decreases NMJ complexity and alters the composition of the postsynaptic density (PSD). Collectively, these data suggest that *Vps54/scat* functions in *Drosophila* larval MNs to control NMJ development and synaptic morphology.

RESULTS

scat is required to control axon terminal growth at the larval NMJ

To determine whether *scat* has a function in fly MNs, we examined the development of a well-characterized NMJ in third instar larvae. The classic *scat*^{1} allele is a P-element insertion near the 5′ end of the second coding exon of the *scat* gene (Fig. S1) (Castrillon et al., 1993). Protein expression is completely disrupted in testes of *scat*^{1} homozygotes suggesting that it is a null allele (Fári et al., 2016). Using quantitative real-time PCR (qPCR), we have confirmed that expression is disrupted in the larval CNS of *scat*^{1} mutants (Fig. S1B). We found that the morphology of the NMJ was distinctly different in *scat*^{1} mutants compared to controls (Fig. 1A). Quantitative analysis of the number of type 1 synaptic boutons revealed a greater than twofold overelaboration in *scat*^{1} null animals (Fig. 1B; 114% increase; $P<0.0001$). A similar phenotype was observed when the *scat*^{1} allele was placed in *trans* to the overlapping *Df(2L)Exel8022* deficiency (Fig. 1A,B; 94% increase; $P<0.0001$). Quantification of the number of synaptic arbor branch points correlated strongly with synaptic boutons (Fig. 1C). The *scat*^{1} homozygous mutant phenotype was rescued when a transgenic construct was introduced back into the *scat*^{1} background (Fig. 1A–C). This rescue transgene includes the minimal *scat* promoter and ∼350 bp of upstream genomic DNA controlling the expression of a hemagglutinin (HA)-tagged *scat* cDNA (*scat-HA:scat*) and restores Scat expression in the larval CNS (Fig. S1B). Taken together, these data suggest that *scat* has a critical function in the control of axon terminal growth during larval NMJ development.

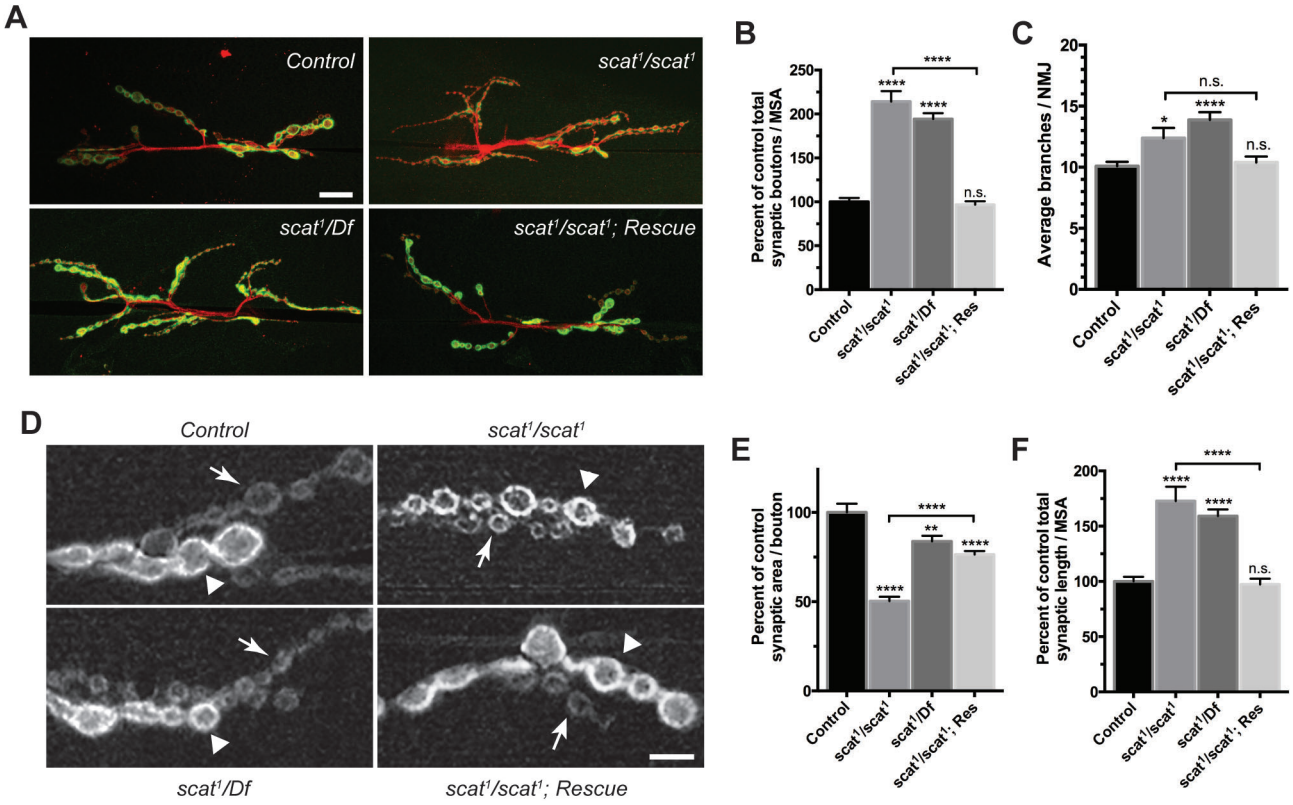

Fig. 1. *scat* is a negative regulator of synaptic development at the larval NMJ. (A) *scat* loss-of-function causes defects in NMJ structure. Wandering third instar larvae from controls, *scat*^{1} homozygotes, *scat*^{1}*/Df(2L)Exel8022*, and the *scat*^{1}*/scat*^{1}*; scat-HA:scat/scat-HA:scat* rescue (Res) lines were stained with antibodies targeting the postsynaptic density marker, Dlg (green) and the neuronal membrane marker, HRP (red). Images show maximum Z-projections. The NMJs innervating body wall muscles 6/7 in abdominal segment 3 (m6/7 in A3) were analyzed. *scat* mutants have an increased number of boutons and synaptic arbors in comparison to controls. Scale bar: 20 µm. (B) Total bouton number/MSA (normalized to control) and (C) synapse branch points are significantly increased in *scat* mutants. Both were quantified by counting manually and both phenotypes are rescued by the introduction of the *scat-HA:scat* transgenic construct. *N*=23, 21, 24 and 25. (D) *scat* loss-of-function causes defects in the size of both type 1b (arrowhead) and 1s boutons (arrows). Wandering third instar larvae from controls, *scat*^{1} homozygotes, *scat*^{1}*/Df(2L)Exel8022*, and the *scat*^{1}*/scat*^{1}*; scat-HA:scat/scat-HA:scat* rescue lines were stained with an antibody targeting Dlg. Images shown are single focal planes through the equator of the type 1b boutons. *scat*^{1} homozygotes have noticeably smaller boutons than controls. The NMJs innervating muscle 6/7 in body segment A3 were analyzed. Scale bar: 5 µm. (E) Total synaptic length/MSA (normalized to control) is significantly increased and (F) synaptic area per bouton is decreased in *scat*^{1} homozygotes. Both features were quantified using the Morphometrics algorithm. *N*=23, 19, 24 and 25. Data are represented as the mean±s.e.m. All statistical analysis was done by Kruskal–Wallis followed by a Dunn's multiple comparison test. Unless otherwise indicated, all comparisons have been made to the control. **P*<0.05, ***P*<0.01, *****P*<0.0001.

Biology Open (2020) 9, bio053421. doi:10.1242/bio.053421

During our NMJ analyses, we noted that synaptic bouton morphology appeared to also be abnormal in *scat*^{1} mutants. The NMJ at muscle 6/7 has two types of synaptic boutons – type 1b (big) and type 1s (small) boutons, which are derived from two distinct MNs and differ in morphology and physiology (Menon et al., 2013). Immunostaining of Discs large (Dlg), the fly ortholog of the postsynaptic density protein, PSD-95, is also usually stronger in in type 1b boutons and weaker in type 1s boutons (Lahey et al., 1994). In contrast to controls, Dlg staining in *scat*^{1} homozygotes is roughly the same in both types of boutons and is spotty and discontinuous suggesting that localization of Dlg to postsynaptic densities may be partially disrupted (Fig. 1D). Additionally, both types of boutons were smaller in *scat*^{1} mutants (Fig. 1D). Quantification of this revealed a significant twofold decrease in synaptic area per bouton and an increase in total synaptic length in *scat*^{1} homozygotes (Fig. 1E,F; area=50% of controls; P<0.0001; length=173% of controls; P<0.0001). In contrast, a robust a reduction in bouton size was not seen in *scat*^{1}/*Df* larvae (Fig. 1E). However, the deficiency line deletes the *scat* gene region plus about 60 kb of flanking sequence including nine neighboring genes. It is possible that heterozygosity of one or more of these loci might have an uncharacterized effect on NMJ growth. Both the 'small bouton' and length phenotypes were rescued by the *scat-HA:scat* transgene (Fig. 1E,F).

scat function is required in both the MN and muscle to control NMJ development

Given the critical role of *Vps54* in mouse MNs, we postulated that *scat* might have an important presynaptic function at the larval NMJ. To investigate this, we targeted the knockdown of *scat* expression in MNs using a transgenic short hairpin RNA (shRNA) driven by the MN-specific *C380-Gal4* driver. This *scat shRNA* transgene reduced levels of *scat* mRNA in the CNS by about 50% (Fig. S1C). Presynaptic knockdown of *scat* resulted in a highly significant increase in the number of boutons (Fig. 2A,B; 81% increase; P<0.0001). To confirm these results, we drove expression

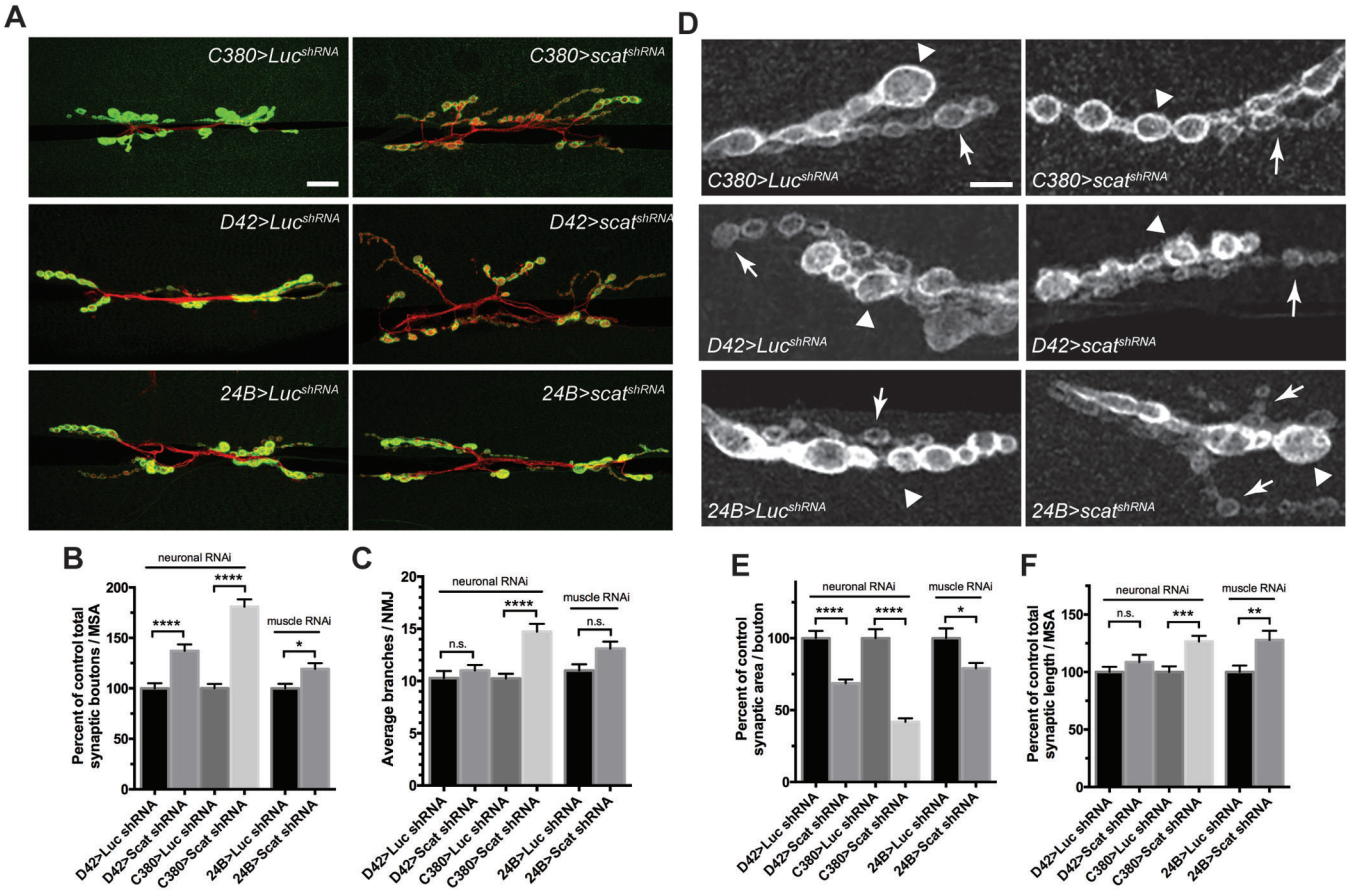

Fig. 2. *scat* has a presynaptic function in the control of NMJ development. (A) Knockdown of *scat* expression in the presynaptic motor neuron by RNAi causes defects in NMJ structure. An inducible transgenic shRNA targeting luciferase (*UAS-LUC.VALIUM10*) or *scat* (*UAS-TRiP*^{HMS01910}) was expressed in motor neuron using the *C380-Gal4* or the weaker *D42-Gal4* driver or in muscle using *24B-Gal4*. NMJs at muscle 6/7 in body segment A3 in late third instar larvae were stained with antibodies targeting Dlg (green) and HRP (red). Images show maximum Z-projections. Presynaptic knockdown of *scat* causes an increased number of boutons and synaptic arbors. Scale bar: 20 µm. (B) As in *scat* mutants, the total bouton number/MSA (normalized to the respective control) and (C) synapse branch points are significantly increased by presynaptic *scat* knockdown. *N*=18, 18, 17, 18, 20 and 25. (D) Presynaptic *scat* knockdown causes defects in the size of type 1b (arrowhead) and 1 s boutons (arrows). Wandering third instar larvae from genotypes indicated in A were stained with an antibody targeting Dlg. Images show single focal planes through the equator of type 1b boutons. Presynaptic *scat* knockdown causes a reduction in the size of type 1 boutons. Scale bar: 5 µm. (E) As in *scat* mutants, total synaptic area per bouton/MSA (normalized to control) is significantly decreased and (F) length is increased by presynaptic *scat* knockdown. Effects are statistically significant but not as dramatic following *scat* RNAi in the postsynaptic muscle. Both features were quantified using the Morphometrics algorithm. *N*=18, 17, 17, 18, 20 and 19. All statistical comparisons shown have been compared to driver-specific controls (*driver*/+ heterozygotes) using a two-tailed Mann–Whitney *U*-test. Data represented as the mean±s.e.m. *P<0.05, **P<0.01, ***P<0.001, ****P<0.0001.

Biology Open (2020) 9, bio053421. doi:10.1242/bio.053421

of the shRNA transgene using a second, albeit weaker, MN driver, *D42-Gal4*, and observed a similar increase in the number of synaptic boutons (Fig. 2A,B; 37% increase; $P<0.0001$). To determine if the function of *scat* was restricted to the MN, we examined targeted knockdown of *scat* expression in larval muscle using the muscle-specific driver *24B-Gal4* (Fig. 2A,B). Knockdown in the postsynaptic muscle also resulted in a small but significant increase in bouton number relative to controls (Fig. 2B; 19% increase; $P=0.0207$). As in $scat^{1}$ mutants presynaptic knockdown of *scat* also caused a significant increase in the number of synaptic arbor branches (Fig. 2C; *C380>scat shRNA*; $P<0.0001$). Collectively, these data suggest that *scat* functions in both the pre- and postsynaptic compartments to control NMJ development.

We were also interested to see if bouton morphology was altered by pre- or postsynaptic disruption of *scat* expression. While the small bouton phenotype was not as obvious in either case (Fig. 2D), presynaptic RNAi does significantly reduce bouton size. *C380>scat shRNA* caused a 58% reduction in synaptic area per bouton (Fig. 2E; $P<0.0001$). A similar result was observed using the *D42-Gal4* driver (Fig. 2E; 41% decrease; $P<0.0001$). *C380>scat shRNA* also had a modest but significant effect on total NMJ length (Fig. 2F; 27% increase; $P=0.0006$). As seen in $scat^{1}$ mutants, knockdown of *scat* in motor neurons (but not in muscle) partially disrupted normal Dlg expression and localization to postsynaptic densities (Fig. 2D). Disruption of *scat* expression in the muscle also had a significant effect on average bouton size (Fig. 2E; 21% decrease; $P=0.0303$) and length of NMJs (Fig. 2F; 28% increase; $P=0.0043$). Together, these data suggest that *scat* is required on both sides of the synapse to control bouton morphology.

Conversely, we asked if *scat* overexpression impacted NMJ development. To test this, we constructed a fly line containing a Gal4-inducible version of the HA-tagged *scat* cDNA (*UAS-HA:scat*). The global overexpression of HA:Scat in a wild-type background (*tub-Gal4>UAS-HA:scat*) had no impact on NMJ development (Fig. S2). Neuronal expression of *UAS-HA:scat* with a strong pan-neuronal driver (*elav-Gal4*) caused a small but statistically significant increase in branching and synaptic area per bouton (Fig. S2; branching, $P=0.0159$; synaptic area, 21% increase; $P=0.0008$). In contrast, overexpression using a strong muscle driver (*Mef2-Gal4*) resulted in a significant increase in branch and synaptic bouton number with no changes in bouton morphology (Fig. S2; branching, $P=0.0072$; bouton number, 25% increase, $P=0.0003$). Together, these data suggest that both loss- and gain-of-function of *scat* causes NMJ defects.

Scat localizes to the *trans*-Golgi in MNs, glia and muscle cells

Vps54 localizes primarily to the TGN in yeast and in mouse spermatids (Berruti et al., 2010; Conibear and Stevens, 2000). Similar localization patterns have been observed with fluorescently-tagged Scat protein in *Drosophila* testes (Fári et al., 2016). Based on this, we predicted that Scat would localize to the TGN in larval MNs and muscle cells. In our hands, the only available antibody targeting Scat did not work in neurons for immunofluorescence. Moreover, HA-tagged Scat expression from two copies of the *scat-HA:scat* transgene could not be detected. Therefore, to examine subcellular localization, we drove expression of *UAS-HA:scat* using the ubiquitous *tub-Gal4* driver and labeled the HA:Scat protein using an anti-HA antibody. First, we counterstained with an antibody that recognized the golgin Lava lamp (Lva), a marker for the *cis*-Golgi (Sisson et al., 2000). We found that most overexpressed HA:Scat was juxtaposed to Lva staining in the soma of larval MNs (Fig. 3A), the ensheathing glial cells surrounding peripheral nerves (Fig. 3B), and in body wall muscle (Fig. 3C). Both HA:Scat and Lva were absent from motor axons (blue in Fig. 3B) and presynaptic boutons (grey in Fig. 3C). Taken together, these data are consistent with HA:Scat localizing to a structure in close proximity to the *cis*-Golgi.

Because of the strong presynaptic role for *scat* in the control of NMJ development, we focused on further characterizing the subcellular localization of overexpressed Scat within MNs. To confirm localization of Scat to the TGN, we counterstained with an antibody targeting *Drosophila* Syntaxin-16 (dStx16), a core component of the t-SNARE that is involved in retrograde transport of endosome-derived vesicles to the TGN (Amessou et al., 2007; Quenneville et al., 2006). As expected, HA:Scat colocalized strongly with dStx16-positive foci in the MN cell bodies [Fig. 3D–G; Pearson's correlation coefficient (PCC)=0.55±0.02]. This is consistent with the localization of Scat to the TGN and near the t-SNARE complex. In yeast, Vps54 also localizes to EEs via a conserved C-terminal domain and it is required for retrograde transport from EEs to the TGN (Quenneville et al., 2006). To examine the colocalization of HA:Scat with endosomal compartments, we counterstained larval MNs with antibodies targeting the small GTPases, Rab5, Rab7 and Rab11, which are used as markers for EEs, LEs and recycling endosomes (REs), respectively. In contrast to dStx16, we observed a low degree of colocalization between HA:Scat and Rab5, Rab7, or Rab11 (Fig. 3H–S; PCC=0.15±0.01, 0.22±0.04, and 0.178±0.02). Interestingly, HA:Scat does sometimes appear to localize to a structure immediately adjacent to Rab5-positive EEs (arrows in Fig. 3K). We cannot rule out that this is due to the high-density of Rab5-positive structures in larval MNs. However, a similar result was not observed with either Rab7- or Rab11-postive endosomes with similarly high numbers of foci (Fig. 3O,S).

Localization of syntaxin-16 to the TGN is partially disrupted in *scat* mutant MNs

Endosomal trafficking is required for the bi-directional transfer of membranes and receptors along axons and dendrites, which is likely to be important in regulating different aspects of synaptic development (Lasiecka and Winckler, 2011). To begin to understand how loss of *scat* expression in larval MNs leads to synaptic overgrowth, we analyzed the impact on the localization of markers for endocytic trafficking pathways. In yeast and mammalian cells, GARP is required to tether vesicles derived from EEs and LEs to the TGN (Conboy and Cyert, 2000; Conibear and Stevens, 2000). It does so, in part, by controlling the assembly of the t-SNARE complex (Pérez-Victoria and Bonifacino, 2009). Based on this, we asked if dStx16 localization would be disrupted in *scat* loss- or reduction-of-function mutant MNs. As predicted, dStx16 antibody staining was more diffuse in $scat^{1}$ homozygous larvae (Fig. 4A). This was rescued by the introduction of the *scat-HA:scat* transgene. Very similar results were seen following targeted disruption of *scat* expression in larval MNs by RNAi (Fig. 4A). However, punctate dStx16 fluorescence remains in *scat* mutants and after Scat RNAi suggesting that this phenotype is only partially penetrant. Together, these data indicate that *scat* contributes to dStx16 localization or membrane association at the TGN. Moreover, this suggests that localization of an integral component of the retrograde trafficking pathway (the t-SNARE complex) has been partially disrupted.

Next, we determined if *scat* loss-of-function had an impact on endosomal pools in MNs. Disruption of *Vps54* expression in yeast causes the accumulation of vesicles containing markers for EEs (Quenneville et al., 2006). In contrast, MNs in the wobbler mouse

Biology Open (2020) 9, bio053421. doi:10.1242/bio.053421

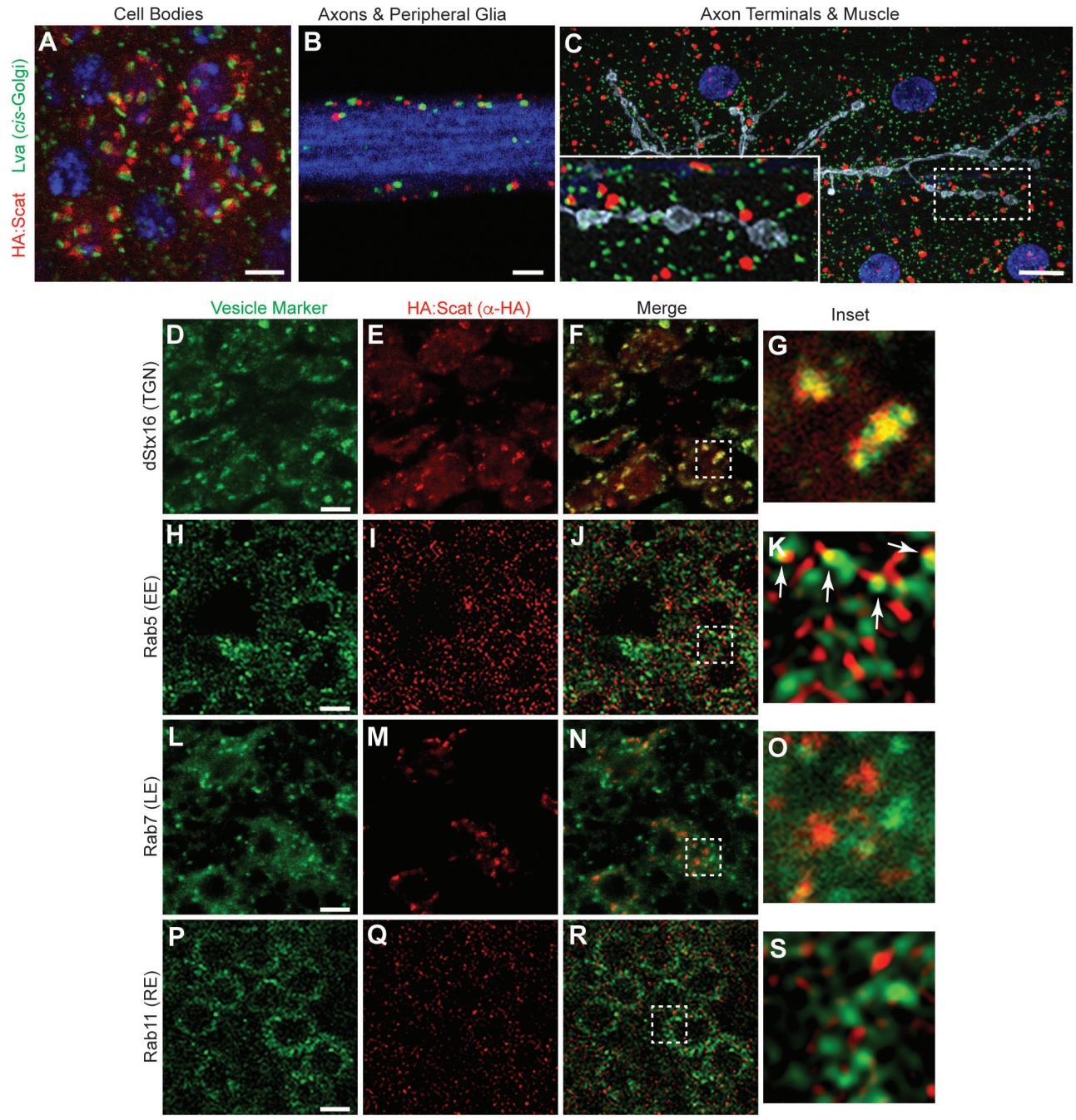

Fig. 3. Scat localizes to the TGN in MN cell bodies. (A–C) Scat localizes to a structure adjacent to the *cis*-Golgi in (A) motor neuron cell bodies, (B) peripheral glia, and (C) body wall muscle. (A,B) Ventral ganglia and (C) body wall muscle preps from wandering third instar larvae expressing inducible *HA:scat* under control of the *tubulin-Gal4* driver were stained with antibodies targeting the HA tag (red) and the *cis*-Golgi marker, Lva (green). Single focal planes are shown in A and B while C is a maximum Z-projection. HA:Scat localizes to the motor neuron cell body but not peripheral axons or axon terminals. Most HA-positive structures are adjacent to the Lva-positive *cis*-Golgi. Blue is DAPI (DNA) in A and C and Hrp (axon) in B. Grey in C is Hrp (axon). Scale bars are 2.5 µm in A and 10 µm in B and C. (D–S) *tub-Gal4>HA:scat* animals were counterstained with antibodies targeting the HA tag (red) and the indicated marker (green). Images shown are single focal planes through MN cell bodies in the larval ventral ganglion. Vesicle trafficking markers shown are the TGN marker, Syntaxin 16 (D–G), the early endosome marker, Rab5 (H–K), the late endosome marker, Rab7 (L–O), and the recycling endosome marker, Rab11 (P–S). Larvae showing the colocalization of HA:Scat with Rab5 and Rab11 were fixed with Bouin's reagent, which provided much better signal to noise. Larvae showing HA:Scat with dStx16 and Rab7 were fixed with paraformaldehyde. The boxed areas indicated in the merged images (F, J, N and R) are shown in G, K, O and S (respectively). The arrows shown in K are indicating localization of HA:Scat in spots immediately adjacent to Rab5. Scale bars in D, H, L and P are 2.5 µm.

appear to accumulate large Rab7-positive LEs (Palmisano et al., 2011). To determine if endosomal trafficking is affected by the disruption of *scat* expression, we examined the localization of markers for EEs and LEs in larval MNs using monoclonal antibodies targeting Hrs and Rab7, respectively (Riedel et al., 2016). Surprisingly, neither the size or number of Hrs- and Rab7-postive endosomes were obviously altered in $scat^{1}$ homozygous mutant larvae (Fig. 4B,C). Similar results were observed with a

Biology Open (2020) 9, bio053421. doi:10.1242/bio.053421

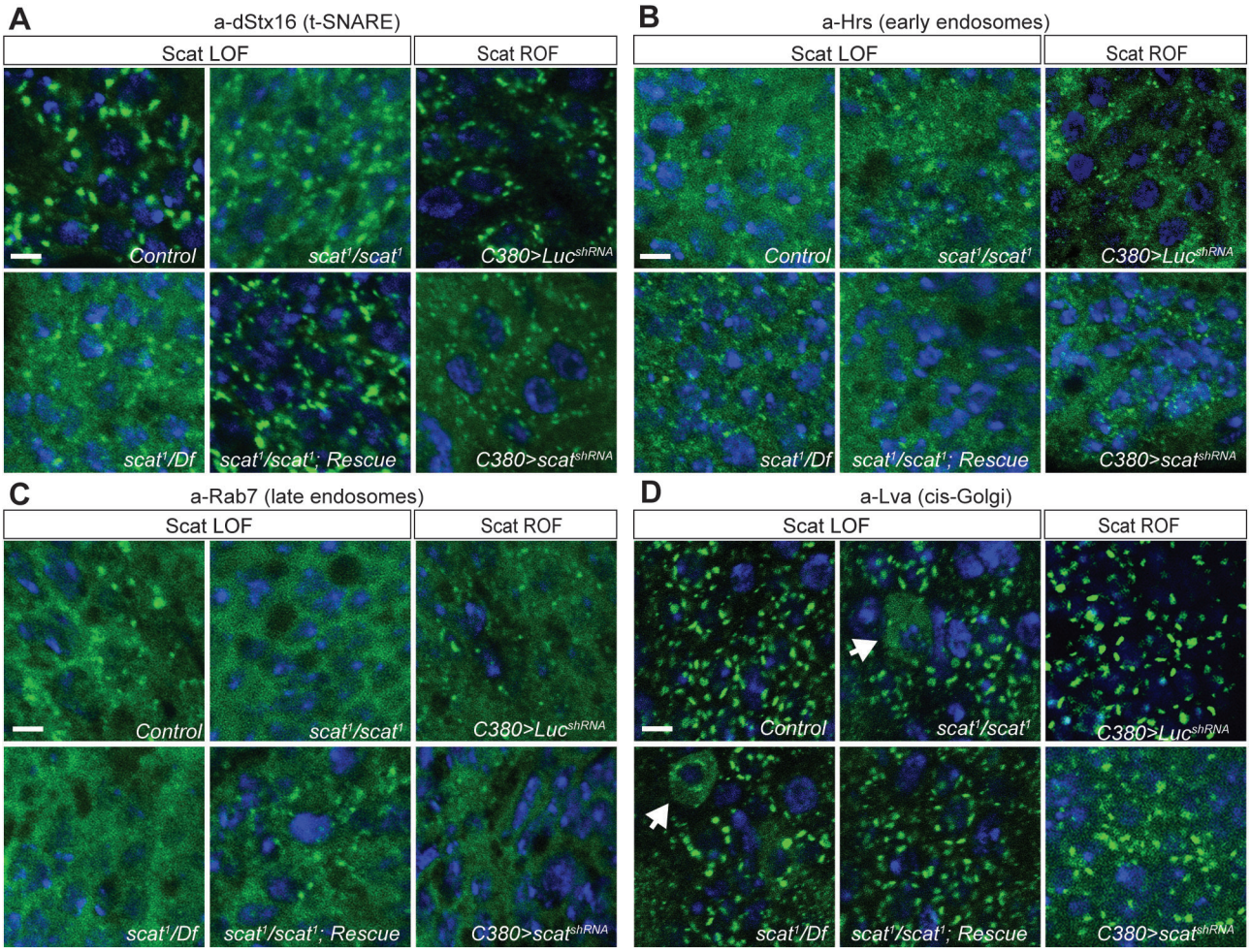

Fig. 4. *scat* mutant MNs have defects in Syntaxin-16 localization and *cis*-Golgi integrity. (A) Localization of Syntaxin-16 to the TGN is disrupted in *scat*^{1} mutants. Images shown are single focal planes. Ventral ganglia from wandering third instar larvae from controls, *scat*^{1} homozygotes, *scat*^{1}*/Df(2L)Exel8022*, and the *scat*^{1}*/scat*^{1}*; scat-HA:scat/scat-HA:scat* rescue lines were stained with an antibody targeting (A) dStx16 (green) and DAPI to visualize nuclei (blue). dStx16 staining is significantly more diffuse (but still clearly punctate) in *scat*^{1} mutants compared to controls. The *scat*^{1} mutant phenotype is rescued by the introduction of the *scat-HA:scat* transgene. Similar results were observed in *C380>scat shRNA* MNs. (B) EEs are not affected in *scat*^{1} mutants. The indicated genotypes were stained with an antibody targeting the EE- and multivesicular body-associated protein, Hrs (green) and DAPI (blue). (C) LEs are not affected in *scat* mutants. The indicated genotypes have been stained with an antibody targeting Rab7 (green) and DAPI (blue). (D) Localization of the *cis*-Golgi marker, Lva is partially disrupted in the cell body of some *scat* mutant and motor neurons (arrows). The indicated genotypes have been stained with an antibody targeting Lva (green) and DAPI (blue). This phenotype is never observed in control or rescue larvae. More global effects are observed in *C380>scat shRNA* MNs. Scale bars: 2.5 µm.

second set of antibodies targeting both Rab5 and Rab7 (Fig. S3). Thus, at least at this stage of development, disruption of *scat* does not have a visible impact on endosomal populations.

Although *Vps54* loss-of-function in cultured mammalian cells causes defects in vesicle trafficking pathways, there is no apparent impact on Golgi structure or function (Karlsson et al., 2013). In contrast, MNs in the wobbler mouse show signs of Golgi dysfunction and fragmentation beginning in early stages of neurodegeneration (Palmisano et al., 2011). In order to examine Golgi structure after the disruption of *scat* expression, we stained larval MNs with antibodies targeting Lva (Sisson et al., 2000). Interestingly, we found that some MN cell bodies in *scat*^{1} homozygotes and *scat*^{1}*/Df(2L)Exel8022* larvae had diffuse and cytoplasmic Lva staining suggesting that *cis*-Golgi integrity in some neurons has been partially disrupted (Fig. 4D). We never observed this phenotype in controls or transgenic rescue animals (Fig. 4D). We observed a similar phenotype following the targeted depletion of *scat* in larval MNs by RNAi (Fig. 4D). However, in RNAi larvae, Lva staining was globally diffuse and punctate structures remained more intact in affected neurons. Collectively, these data indicate that *scat* expression is required, at least in part, to maintain Golgi integrity in larval MNs. These data also suggest the possibility that the partial disruption of dStx16 in *scat* mutants may be due to a more global Golgi defect.

scat interacts genetically with Rab proteins to control axon terminal growth

We were next interested in gaining mechanistic understanding into how the disruption of *scat* expression in MNs leads to the overgrowth of axon terminals. Rab proteins not only associate with specific endosomal compartments, their activity is also required to mediate all steps of membrane trafficking (Pfeffer, 2017). Rabs function by switching between GDP- and GTP-bound forms, which regulates their ability to bind to specific Rab effector proteins (Pfeffer and Aivazian, 2004). Transgenic *Drosophila* lines have been constructed that contain Gal4-inducible Rabs that are

Biology Open (2020) 9, bio053421. doi:10.1242/bio.053421

GTP-binding defective conferring dominant-negative activity and allow for the cell autonomous disruption of Rab function (Zhang et al., 2007). In our hands, MN-specific expression of wild-type and dominant-negative Rab5, Rab7 and Rab11 had no effect on the number of type 1 synaptic boutons at larval muscle 6/7 compared to controls (Fig. 5A,B). If *scat* interacts genetically with Rab proteins to control synaptic development, we expected that co-expression of wild-type or dominant-negative Rabs would enhance or suppress the *scat* knockdown phenotype. Interestingly, co-expression of both forms of Rab5, Rab7 and Rab11 significantly suppressed the *scat* shRNA overgrowth phenotype. In most cases, these NMJs appeared to be morphologically indistinguishable from negative controls (Fig. 5A). There were two notable exceptions to this. First, co-expression of wild-type Rab5 with the *scat* shRNA often caused the formation of clusters of synaptic boutons instead of the normal 'beads on a string' phenotype (Fig. 5C). Second, in *C380>scat shRNA, Rab7 (DN)* animals, postsynaptic Dlg staining appears to be appreciably disrupted (Fig. 5C). As a result, total bouton number was significantly reduced when compared to *C380>scat shRNA* and *C380>Rab7 (DN)* controls (Fig. 5B; 54% decrease, $P<0.0001$ and 46% decrease, $P<0.0001$, respectively). In summary, these data suggest that the regulation of normal NMJ development by Scat requires the activity of Rab5, Rab7 and Rab11. Disruption of both *scat* and *rab7* function in motor neurons significantly reduced NMJ complexity.

scat interacts genetically with *rab7* to regulate synapse integrity at the larval NMJ

Postsynaptic Dlg staining appears to be partially disrupted in $scat^{1}$ mutants and following presynaptic knockdown by RNAi (Figs 1D and 2D) and the disruption of both *scat* and *rab7* significantly enhances this phenotype (Fig. 5C). At the *Drosophila* NMJ, Dlg forms a multimeric scaffold that is required for the clustering of postsynaptic glutamate receptors (GluRs) containing the GluRIIB subunit but mutations in *dlg* have no effect on the localization of its alternative subunit, GluRIIA (Chen and Featherstone, 2005). Thus, we asked if GluR localization to postsynaptic sites was altered following the disruption of both *scat* and *rab7* function. High resolution, single focal plane images of NMJs confirmed that Dlg staining was reduced and spotty in type 1b synapses in *C380>scat shRNA, Rab7 (DN)* larvae compared to controls (Fig. 6A). Strikingly, staining with GluRIIB antibodies was slightly reduced in *C380>scat shRNA* animals and significantly disrupted in *C380>scat shRNA, Rab7 (DN)* larvae (Fig. 6B). In contrast, the

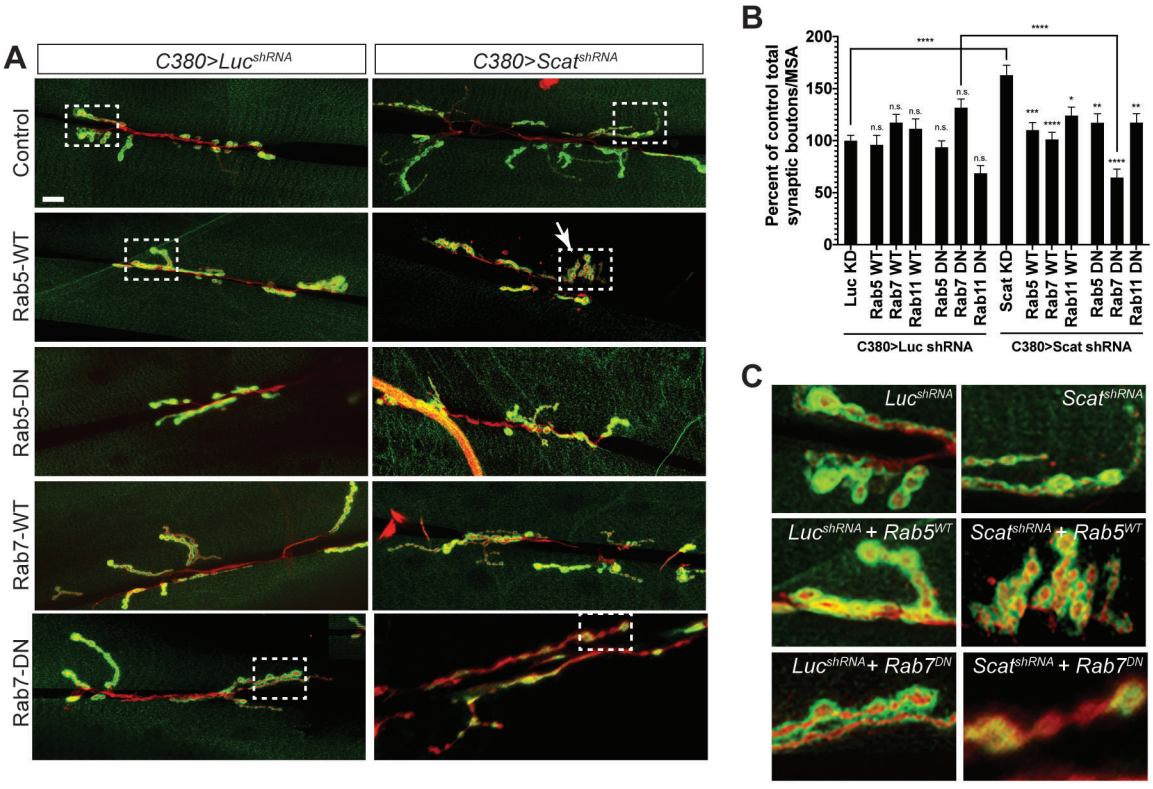

Fig. 5. *scat* interacts genetically with Rab5, Rab7, and Rab11 to control NMJ development. (A) NMJ phenotypes caused by the motor neuron-specific knockdown of *scat* expression by RNAi are suppressed by overexpression of wild-type and dominant-negative transgenes for Rab5, Rab7 and Rab11 (Rab11 images are not shown). An inducible transgenic shRNA targeting luciferase (*UAS-LUC.VALIUM10*) or *scat* ($UAS\text{-}TRiP^{HMS01910}$) was expressed in motor neuron using the *C380-Gal4* driver in combination with an inducible YFP-tagged wild-type or dominant negative Rab5, Rab7, or Rab11 (*UAS-YFP: Rab*). NMJs at muscle 6/7 in body segment A3 in wandering third instar larvae were stained with antibodies targeting Dlg (green) and HRP (red). Images show maximum Z-projections. The boxed areas are blown up in C to show altered synaptic bouton or PSD morphologies. Scale bar: 20 µm. (B) As shown in Fig. 2, the total bouton number/MSA (normalized to the respective control) are significantly increased by presynaptic *scat* knockdown. This phenotype is suppressed by co-expression of wild-type and dominant negative Rabs. *C380>scat shRNA, Rab7 (DN)* double mutant NMJs are significantly smaller. *N*=18, 12, 16, 13, 22, 17, 21, 17, 18, 20, 20, 22, 21 and 23. (C) Boxed areas in A. Many *C380>scat shRNA, Rab5 (WT)* NMJs have a clustered bouton phenotype similar to many endocytic mutants. Dlg staining and bouton morphology is significantly disrupted in *C380>scat shRNA, Rab7 (DN)* double mutants. Data are represented as the mean±s.e.m. Unless otherwise indicated, all comparisons have been made to the control. Statistical analysis was done using a one-way ANOVA followed by a Holm-Sidak multiple comparison test. *$P<0.05$, **$P<0.01$, ***$P<0.001$. ****$P<0.0001$.

Biology Open (2020) 9, bio053421. doi:10.1242/bio.053421

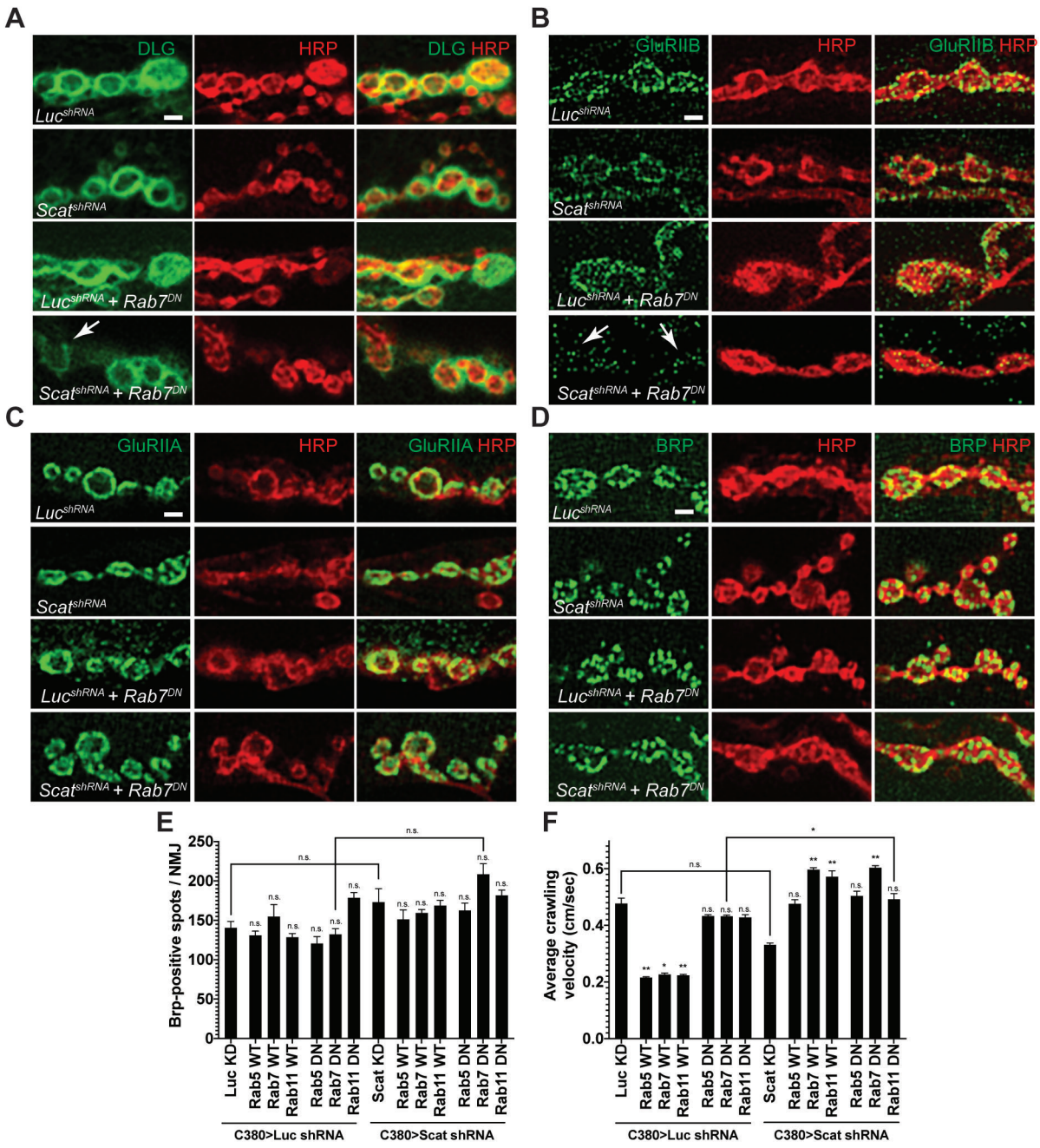

Fig. 6. *scat* interacts genetically with *rab7* to control the composition of the PSD. Localization of the PSD proteins (A) Dlg, (B) GluRIIB, (C) GluRIIA and the AZ marker (D) Brp to synaptic boutons at muscle 6/7 in body segment A3 in late third instar larvae are shown in green. All NMJs have been counterstained with an antibody targeting HRP (red). Merged images are included to confirm pre- or postsynaptic localization. All images are single focal planes. Synaptic bouton structure has been better preserved here using Bouin's fixative. The arrow in A points to a type 1b bouton with abnormally low levels of Dlg and neighboring boutons have spotty Dlg staining. Arrows in B point to synaptic boutons where GluRIIB localization has been significantly disrupted (compare $scat^{shRNA}$, $Rab7^{DN}$ to any of the control genotypes). Scale bar: 2.5 µm. (E) Quantification of the number of Brp-positive spots per NMJ. No significant difference was observed in any genotype (N=5 each). Statistical analysis was done using a one-way ANOVA followed by a Holm-Sidak multiple comparison test. (F) Average crawling velocity of third instar larvae for each genotype (N=10 each). MN-specific overexpression of wild-type Rab5, Rab7 and Rab11 alone significantly suppressed larval crawling velocity while overexpression of dominant negative Rabs had no effect. Overexpression of both wild-type and dominant negative forms of all Rabs suppressed the *C380>Scat shRNA* phenotype. Statistical analysis was done by Kruskal–Wallis followed by a Dunn's multiple comparison test. *P<0.05, **P<0.01.

localization of the GluRIIA subunit does not appear to be affected (Fig. 6C) suggesting that the core GluR has not been lost from postsynaptic sites. We cannot rule out that reduced GluRIIB staining at the NMJ is due to reduced expression. However, these data suggest that the Scat protein is required in the presynaptic cell to regulate the localization of Dlg and GluRIIB to postsynaptic sites via an unknown trans-synaptic mechanism that involves the activity of presynaptic Rab7.

In order to further explore the role of *scat* in synaptic architecture at the NMJ, we next asked if *scat* was required to control the

Biology Open (2020) 9, bio053421. doi:10.1242/bio.053421

localization of Bruchpilot (Brp) to presynaptic boutons. Brp is similar to the human ELKS/CAST family of active zone (AZ) proteins and is required to regulate AZ structure and function at synapses (Wagh et al., 2006). At the larval NMJ, Brp localizes to presynaptic AZs and the lack of Brp causes defects in AZ assembly, Ca^{2+} channel clustering, and vesicle release (Kittel et al., 2006). We observed no significant difference in the total number of Brp puncta per NMJ in *C380>scat shRNA, Rab7 (DN)* larvae or any other genotype tested (Fig. 6D,E). Similar results were observed in $scat^{1}$ homozygotes compared to controls and transgenic rescues (Fig. S4). Instead, we observed a significant decrease in the number of AZs per synaptic bouton, which was partially rescued by the *scat-HA:scat* transgene (Fig. S4; 7.0±0.70 in controls versus 4.5±0.46 in $scat^{1}$ homozygotes, P=0.009; $scat^{1}$ homozygotes versus 5.1±0.41 in $scat^{1}$ homozygotes with two copies of the *scat-HA:scat* transgene, P=0.037). Collectively, these results suggest that presynaptic AZs have not been disrupted.

Because disruption of *scat* expression (either alone or in combination with expression of a dominant-negative *rab7*) causes abnormal NMJ development, we next asked if larval crawling behavior was affected. Defects in larval locomotion have been directly linked to neuronal and synaptic dysfunction (Folwell et al., 2010; Mudher et al., 2004). Comparison of larval crawling speeds showed no statistical difference between *C380>scat shRNA* animals and controls (Fig. 6F). Interestingly, MN-specific expression of wild-type Rab5, Rab7 and Rab11 all significantly decreased larval crawling velocity (55% decease, P=0.0044; 53% decrease, P=0.0173; and 53% decrease, P=0.0184, respectively). However, expression of the dominant-negative forms of these proteins alone had no effect (Fig. 6F). Conversely, MN-specific knockdown of *scat* along with expression of wild-type Rab7, Rab11 and dominant negative Rab7 all significantly increased average crawling velocity compared to *C380>scat shRNA* controls (44% increase, P<0.0001; 72% increase, P=0.0013; and 48% increase P<0.0001, respectively). Thus, there appears to be no correlative relationship between larval crawling behavior and either synapse morphology or postsynaptic density composition in *C380>scat shRNA* and *rab* transgenic animals.

DISCUSSION

The GARP complex is required to control a wide range of cellular processes highlighting the importance of understanding more about its function (Bonifacino and Hierro, 2011). Notably, the disruption of two subunits of GARP have been linked to neuronal dysfunction in mammals: (1) a homozygous recessive mutation in *Vps54* in the wobbler mouse (Schmitt-John et al., 2005), and (2) heterozygous mutations in *Vps53* in pontocerebellar hypoplasia type 2E in humans (Feinstein et al., 2014). Vps54 associates specifically with the GARP complex while Vps53 is a core component of both GARP and the endosome-associated protein (EARP) complex (Schindler et al., 2015). An increased number of swollen Rab7-positive LEs have been reported in both cases. Here, we show that the loss of *scat* expression in larval *Drosophila* MNs appears to have no impact on LE size or number (Fig. 4C; Fig. S3B). Despite this, presynaptic *scat* does interact genetically with *rab7* to control NMJ growth and composition of the PSD (Figs 5 and 6). These data suggest that disruption of both *scat* and *rab7* has a negative effect on synapse integrity.

Our results demonstrate that *Drosophila* Vps54 localizes to the TGN (Fig. 3D–G) and that the localization of dStx16, a core TGN-associated t-SNARE component, has been partially disrupted in *scat* mutant MNs (Fig. 4A). To facilitate the capture of endosome-derived vesicles, the N-terminus of Vps53 and Vps54 interact directly with SNAREs involved in retrograde transport including the t-SNAREs Stx6 and Stx16, as well as the v-SNARE Vamp4 (Pérez-Victoria and Bonifacino, 2009). The reduction of GARP components by RNAi in mammalian cells reduces, but does not prevent, the formation of TGN-associated t-SNARE complexes (Pérez-Victoria and Bonifacino, 2009). Similarly, our data suggests that the disruption of *scat* in larval MNs has only partially compromised t-SNARE assembly or localization. It is possible that the partial disruption of dStx16 localization in *Drosophila* larval MNs is insufficient to cause visible defects in the size, distribution, or number of endosomal pools at this stage. Alternatively, one could speculate that this might represent a bona fide difference between the function of Vps54 in flies and mammals. The latter hypothesis is supported by the fact that *Vps54* loss-of-function is embryonic lethal in mice but only semi-lethal in *Drosophila* (Castrillon et al., 1993; Schmitt-John et al., 2005).

We also demonstrate that some MNs in *scat* loss- and reduction-of-function larvae have defects in the normal localization of the *cis*-Golgi maker Lva, suggesting there is a link between altered retrograde trafficking and Golgi dysfunction (Fig. 4D). Similarly, in yeast and humans, Vps51 interacts with Stx6, although disruption of this interaction in yeast does not cause trafficking defects (Conibear et al., 2003; Siniossoglou and Pelham, 2002). Depletion of the zebrafish *Vps51* ortholog, *fat free*, in intestinal cells disrupts vesicle trafficking and Golgi morphology (Ho et al., 2006). The latter suggests that GARP (or EARP) plays an important role in the control of Golgi structure. Analysis of Golgi morphology in the symptomatic wobbler mouse reveals significant vacuolization of the Golgi in the soma of MNs (Palmisano et al., 2011). Finally, in *Drosophila* post-mitotic spermatids, $scat^{1}$ mutants have defects in the localization of Golgin245, a conserved golgin associated with the TGN, although the *cis*-Golgi marker (the golgin GM130) was unaffected (Fári et al., 2016). Based on this, we cannot rule out that partial Stx16 mislocalization we observed in $scat^{1}$ MNs is not due to a more global defect in the integrity of both sides of the Golgi ribbon. Future studies aimed at elucidating the precise role of *scat* (and by extension the GARP complex) in membrane trafficking and Golgi function in *Drosophila* could resolve this question.

We show here that MN-specific overexpression of wild-type and dominant negative Rabs can modify *scat* mutant phenotypes at the NMJ (Fig. 5). Several of these Rab proteins already have well-established functions in the control of axon growth and synaptogenesis (Wojnacki and Galli, 2016). For example, Rab5 (EEs), Rab7 (LEs), and Rab11 (REs) all traffic in vertebrate axons and have been implicated in the control of axon growth and guidance (Falk et al., 2014; Ponomareva et al., 2016; van Bergeijk et al., 2015). Membrane and transmembrane proteins are transported to axon terminals via a Rab11-dependent mechanism whereas Rab5 and Rab7 are involved in local recycling and retrograde transport back to the soma (Jin et al., 2018; Khodosh et al., 2006). In *Drosophila*, a loss-of-function mutation in Rab5 causes defects in axon elongation in olfactory projection neurons and sensory neurons (Sakuma et al., 2014; Satoh et al., 2008). Furthermore, mutations in Rab7 linked to Charcot-Marie-Tooth2b disease cause axon growth and guidance defects in fly sensory neurons (Ponomareva et al., 2016). Rab11 has been implicated in fly models for neurodegenerative disorders including Alzheimer's disease (AD) and Huntington's disease (HD) (Breda et al., 2015; Dumanchin et al., 1999; Greenfield et al., 2002; Li et al., 2012, 2009a,b, 2010; Richards et al., 2011; Steinert et al., 2012). Moreover, *rab11* mutants have defects at the larval NMJ

Biology Open (2020) 9, bio053421. doi:10.1242/bio.053421

characterized by a significant increase in synaptic bouton number with a clustered phenotype (Khodosh et al., 2006).

Disruption of *scat* expression causes synaptic hyperplasia (Figs 1 and 2). This phenotype is consistent with a role for *scat* in the development but not degeneration of the larval NMJ. We speculate that this is likely because *scat* loss-of-function has little impact on endosomal trafficking at the larval stage. However, when we disrupt both *scat* expression and Rab7 function in MNs, we see a significantly different phenotype. We find that Dlg+ synaptic boutons are appreciably reduced in *C380>scat shRNA, Rab7 (DN)* larvae compared to controls (Fig. 5A,B). These data suggest that NMJs fail to develop normally in double mutant larvae. This phenotype is not unprecedented in *Drosophila* disease models as a prelude to neurodegeneration. Similar synaptic defects have been observed at the larval NMJ in fly models for ALS, AD, Parkinson's disease (PD), and frontotemporal dementia (Shahidullah et al., 2013; West et al., 2015; Zhu et al., 2013). However, further investigation into the processes occurring during metamorphosis and in adults is required to determine if loss or reduction of *scat* results in age-progressive MN degeneration.

Finally, we show that localization of Dlg and GluRIIB to the PSD is altered in *C380>scat shRNA, Rab7 (DN)* double mutants (Fig. 6). There is a growing body of evidence suggesting that presynaptic mechanisms are involved in the regulation of PSD composition at the fly NMJ. For example, presynaptic pMad (phosphorylated Smad) regulates postsynaptic GluRIIA accumulation in PSDs via a noncanonical BMP signaling pathway (Sulkowski et al., 2016). Presynaptic dMon1 also regulates levels of GluRIIA at PSDs via a trans-synaptic mechanism (Deivasigamani et al., 2015). dMon1 is a conserved effector of Rab5 and is involved in the conversion of EEs to LEs by aiding in the recruitment of Rab7 (Poteryaev et al., 2007; Yousefian et al., 2013). It was proposed that dMon1 may be released from boutons (facilitate the release of some unknown factor) in a manner similar to signaling molecules such as Ephrins, Wingless, and Syt4 (Contractor et al., 2002; Korkut and Budnik, 2009; Korkut et al., 2013). While the mechanism involved in our study is unclear, our results set the stage for further work exploring the relationship between membrane trafficking pathways in the presynaptic neuron and trans-synaptic signaling at the NMJ.

MATERIALS AND METHODS

Drosophila genetics

The following lines were obtained from the Bloomington Stock Center: P(PZ)scat^{1}cn^{1}, cn^{1}, Df(2L)Exel8022, UAS-TRiP(HMS01910), UAS-LUC.VALIUM10, tub-Gal4, C380-Gal4, D42-Gal4, 24B-Gal4, UAS-YFP:Rab5, UAS-YFP:Rab5(S43N), UAS-YFP:Rab7, UAS-YFP:Rab7(T22N), UAS-YFP:Rab11, UAS-YFP:Rab11(S25N). The scat^{1}cn^{1} and cn^{1} lines were crossed into w* to normalize the genetic backgrounds. w*; cn^{1} was used as a control to rule out any phenotypes that might be caused by cn^{1} homozygosity in the scat^{1} homozygote. The Df(2L)Exel8022 line deletes the entire scat gene plus about 60 kb of flanking genomic DNA including nine neighboring genes. The Df line does not contain the cn^{1} allele. The UAS-HA:scat line was made by amplifying the scat-RA open reading frame from the LD22446 cDNA (Berkeley *Drosophila* Genome Project) with a 5′ primer containing the HA tag and then cloned into pUAST. The genomic rescue line (scat-HA:scat) was made by amplifying the scat gene and ∼350 nt of upstream and ∼50 nt of downstream genomic DNA with a 5′ primer containing the HA tag and cloned into pCASPR4. Both transgenic fly lines were generated by Bestgene. The UAS-HA:scat (tub-Gal4>UAS-HA:scat) and scat-HA:scat constructs rescued both scat^{1} semi-lethality and male sterility (data not shown). All fly lines and crosses were maintained on standard Bloomington media in a diurnal 25°C incubator. Statistical analysis was done using larvae from each genotype raised under identical conditions.

Immunohistochemistry and confocal microscopy

Larval body wall preps for NMJ and muscle analysis were dissected in Ca^{2+}-free HL3 saline. Unless otherwise indicated, larvae were immunostained as previously described (Nesler et al., 2016). For imaging of the CNS, larval ventral ganglia and proximal axons were explanted and fixed in 4% paraformaldehyde in PBS. For GluRIIA and GluRIIB (and specific experiments with Rab and DLG) antibodies, larvae were fixed with Bouin's solution for 10 min. Bouin's solution significantly improved signal-to-noise with the anti-HA, Rab5, and Rab11 antibodies but was not compatible with the anti-Rab7 and dStx16 antibodies. All were blocked in PBS containing 0.3% Triton X-100 (PBST), 2% BSA, and 5% normal goat serum for 30 min before incubation overnight with primary antibodies diluted in block. Following washes in PBST, CNS samples were incubated overnight with the appropriate secondary antibodies. All were mounted in DAPI Fluoromount G (Southern Biotech) for confocal microscopy. Primary antibodies used were anti-HA (1:1000) (Sigma-Aldrich; 3F10), Lva (1:50) (Sisson et al., 2000), Stx16 (1:500) (Abcam; ab32340), Dlg (1:100) (DSHB; 4F3), Hrs (1:100) (DSHB; 27-4), Rab5 (1:800) and Rab11 (1:4000) (Tanaka and Nakamura, 2008), Rab7 (1:1500) (DSHB), GluRIIA (1:1000) and GluRIIB (1:1000) (Ramos et al., 2015), Brp (1:1000) (DSHB; nc82), and Dylight 649 anti-HRP (1:1000) (Jackson Labs). The Rab7 and Hrs antibodies were deposited to the DSHB by S. Munro (Riedel et al., 2016), Dlg by C. Goodman (Parnas et al., 2001), and Brp by E. Buchner (Wagh et al., 2006). Anti-mouse and rabbit secondary antibodies were conjugated to Alexa 488, 568, and 633 (Molecular Probes). All imaging was done on an Olympus FV1000 or FV3000 scanning confocal microscope with 40×, 60×, or 100× objectives (N.A. 1.30, 1.42, and 1.40, respectively). When shown, maximum Z projections were assembled from 0.4 µm optical sections using Olympus FV software. All image post-processing was done using Adobe Photoshop or ImageJ2 in open-source Fiji (Schindelin et al., 2012, 2015). For colocalization analysis, between three and eight images were examined per experiment. Images were manually thresholded and the Pearson Correlation coefficients calculated using the JACoP plugin for ImageJ2/Fiji (Bolte and Cordelieres, 2006).

Analysis of bouton number, synapse morphology, and active zones

The number of type 1 synaptic boutons were manually counted at muscles 6 and 7 (m6/7) in abdominal segment 3 (A3) as previously described (Pradhan et al., 2012). A synaptic bouton was considered to be a distinctive swelling at the NMJ marked by the presence of both the neuronal membrane marker, Hrp, and the postsynaptic density protein, Dlg (Menon et al., 2013). Boutons were quantified by counting the number of Hrp+ and Dlg+ synapses at each NMJ. To account for differences between genotypes in the scaling of NMJs to muscle size, synaptic bouton numbers were normalized to muscle surface area (MSA). MSA was calculated using ImageJ2/Fiji from images of m6/7 obtained using a 20× objective (N.A. 0.85). Branching was determined by counting branch points between strings of boutons at least three boutons long. The same NMJs were subjected to analysis using the Morphometrics algorithm, A Fiji-based macro that quantifies morphological features of *Drosophila* synapses (Nijhof et al., 2016). The parameters examined here include total bouton counts, NMJ area, and NMJ length. To validate these results, we compared bouton number determined by the macro with manual counts for *scat* mutant analysis.

While total bouton numbers were not identical, macro counts correlated significantly with manual counts (Pearson correlation coefficient=0.76; C.I. 95% 0.66-0.84; P<0.0001; n=91 NMJs). Analysis was done using Fiji version 2.0.0 and the NMJ Morphometrics plugin version 20161129. Settings used were maxima noise tolerance=500, small particle size=10, minimum bouton size=10, and rolling ball radius=500. NMJ outline and skeleton thresholds were set to 'triangle'.

To quantify active zone number, NMJs were counterstained with antibodies targeting Brp and HRP as described above. Maximum Z-projections were processed using the TrackMate plugin for ImageJ2/Fiji (Tinevez et al., 2017). Active zone images were opened in TrackMate using the default calibration settings for the Brp channel. The following additional settings were used: LoG detector=on, estimated blob diameter=1 µm, and threshold settings=100. The results were previewed to ensure accurate detection of found spots and data recorded for all boutons.

Behavioral analysis

For the analysis of larval crawling, videos were collected using an iPhone XR (Apple) set in time-lapse video mode (2 frames per second). Ten larvae were collected for each genotype and transferred to the center of a room temperature 15 cm petri dish containing 2% agarose. 45–90 s videos of each larva were collected in triplicate. Videos were trimmed to 90 frames using the Apple photo editing trimming tool selecting for direct path larval movement away from the edge of the petri dish. Files were then converted from .MOV to .TIF series using the export function in ImageJ2/Fiji. Subsequent analysis was done using TrackMate, a Fiji-based macro developed for single particle tracking (Tinevez et al., 2017). Images were adjusted to maximize contrast between larva and the background. The parameters were adjusted as follows to analyze larval locomotion. Settings used were: LoG detector, HyperStack displayer, simple LAP tracker, and spot tracking were all turned on. The average velocity was recorded for each replicate.

Analysis of *scat* expression by quantitative real-time PCR (qRT-PCR)

For qRT-PCR analysis, seven larval ventral ganglia from each genotype were explanted and homogenized in TRIzol reagent (Invitrogen) and total RNA was isolated using a Direct-zol RNA purification kit (Zymogen). RNA concentration and quality were determined using a RNA IQ Assay Kit (Qubit) and a Quibit 4 Fluorometer. RNA quality scores were all above 9.2 indicating that all samples contained high-quality and undegraded RNA. cDNA was synthesized from 1 µg of total RNA for each genotype using a double-primed RNA to cDNA EcoDry premix (Clontech). qPCR primers were designed using Primer3 software to amplify a ∼150 nt amplicon near the 3′ end of the *scat* mRNA (Fig. S1A). As an internal reference gene, primers were designed to amplify an amplicon of similar size in the housekeeping gene encoding for ribosomal protein S3 (RpS3). This protein is a core component of the small ribosomal subunit. qRT-PCR was conducted on an iQ5 Real Time PCR System (Bio-Rad) using the SsoAdvanced Universal SYBR Green Supermix (Bio-Rad). Three technical replicates were done for each genotype. Melt curve analysis was done at the end of each run and indicated that neither primer set amplified non-specific products. Threshold cycle (C_t) values for each sample were selected by the iQ5 software. The analysis of differential fold change was done using the Livak ($\Delta\Delta C_t$) method (Livak and Schmittgen, 2001).

Primer sequences

The sequences of primers used to generate the *UAS-HA:scat* (inducible) and *scat-HA:scat* (genomic rescue) constructs and for qRT-PCR analysis are listed in Table S1.

Statistics

All data was recorded in Excel (Microsoft) and graphed and analyzed in Prism (GraphPad). Results were considered to be statistically significant at $P<0.05$. Results shown throughout the study are mean±s.e.m. n.s.=not significant, *$P<0.05$, **$P<0.01$, ***$P<0.001$, and ****$P<0.0001$. Data for $scat^1$ loss-of-function and larval crawling velocity were both analyzed by Kruskal–Wallis followed by a Dunn's multiple comparison test to determine significance. Each *scat* RNAi experiment had its own control and was analyzed using a Mann–Whitney *U*-test. The number of synaptic boutons and Brp-positive AZs in genetic interaction experiments were both analyzed by one-way ANOVA followed by a Holm-Sidak multiple comparison test.

Acknowledgements

Some fly strains were from the Bloomington *Drosophila* Stock Center, which is funded by National Institutes of Health grant P40OD018537. The scat-RA cDNA was obtained from the *Drosophila* Genomics Resource Center, which is supported by National Institutes of Health grant P40OD010949. Some antibodies were supplied by the Developmental Studies Hybridoma Bank, which was created by the National Institute of Childhood Health and Development and maintained by the University of Iowa. The Lva antibody was a gift from John Sisson and Christine Fields (Harvard). Rab5 and Rab11 antibodies were provided by Akira Nakamura (Institute of Molecular Embryology and Genetics). The GluR antibodies were a gift from Mihaela Serpe (NIH/NICHD).

Competing interests

The authors declare no competing financial interests.

Author contributions

Conceptualization: P.H.P., E.C.W., E.L.S., M.R.M., J.T.B., S.A.B.; Methodology: P.H.P., E.C.W., E.L.S., M.R.M., J.T.B., S.A.B.; Formal analysis: P.H.P., E.C.W., E.L.S., M.R.M., S.A.B.; Investigation: P.H.P., E.C.W., E.L.S., M.R.M.; Writing - original draft: S.A.B.; Writing - review & editing: E.C.W., J.T.B., S.A.B.; Visualization: P.H.P., E.C.W., E.L.S., M.R.M.; Project administration: S.A.B.; Funding acquisition: J.T.B., S.A.B.

Funding

This work was supported in part by National Institutes of Health Awards [R15 MH114019 to S.A.B. and R15 GM126422 to J.T.B.]. P.H.P. was supported by a Renew DU Postdoctoral Fellowship awarded to S.A.B. and J.T.B. The work was also supported by a pilot grant from the Knoebel Institute for Healthy Aging at the University of Denver awarded to S.A.B.

Supplementary information

Supplementary information available online at
https://bio.biologists.org/lookup/doi/10.1242/bio.053421.supplemental

References

Amessou, M., Fradagrada, A., Falguières, T., Lord, J. M., Smith, D. C., Roberts, L. M., Lamaze, C. and Johannes, L. (2007). Syntaxin 16 and syntaxin 5 are required for efficient retrograde transport of several exogenous and endogenous cargo proteins. *J. Cell Sci.* **120**, 1457-1468. doi:10.1242/jcs.03436

Berruti, G., Ripolone, M. and Ceriani, M. (2010). USP8, a regulator of endosomal sorting, is involved in mouse acrosome biogenesis through interaction with the spermatid ESCRT-0 complex and microtubules. *Biol. Reprod.* **82**, 930-939. doi:10.1095/biolreprod.109.081679

Bolte, S. and Cordelières, F. P. (2006). A guided tour into subcellular colocalization analysis in light microscopy. *J. Microsc.* **224**, 213-232. doi:10.1111/j.1365-2818.2006.01706.x

Bonifacino, J. S. and Hierro, A. (2011). Transport according to GARP: receiving retrograde cargo at the trans-Golgi network. *Trends Cell Biol.* **21**, 159-167. doi:10.1016/j.tcb.2010.11.003

Breda, C., Nugent, M. L., Estranero, J. G., Kyriacou, C. P., Outeiro, T. F., Steinert, J. R. and Giorgini, F. (2015). Rab11 modulates alpha-synuclein-mediated defects in synaptic transmission and behaviour. *Hum. Mol. Genet.* **24**, 1077-1091. doi:10.1093/hmg/ddu521

Castrillon, D. H., Gonczy, P., Alexander, S., Rawson, R., Eberhart, C. G., Viswanathan, S., Dinardo, S. and Wasserman, S. A. (1993). Toward a molecular-genetic analysis of spermatogenesis in drosophila-melanogaster - characterization of male-sterile mutants generated by single P element mutagenesis. *Genetics* **135**, 489-505.

Chen, K. Y. and Featherstone, D. E. (2005). Discs-large (DLG) is clustered by presynaptic innervation and regulates postsynaptic glutamate receptor subunit composition in Drosophila. *BMC Biol.* **3**, 1. doi:10.1186/1741-7007-3-1

Conboy, M. J. and Cyert, M. S. (2000). Luv1p/Rki1p/Tcs3p/Vps54p, a yeast protein that localizes to the late Golgi and early endosome, is required for normal vacuolar morphology. *Mol. Biol. Cell* **11**, 2429-2443. doi:10.1091/mbc.11.7.2429

Conibear, E. and Stevens, T. H. (2000). Vps52p, vps53p, and vps54p form a novel multisubunit complex required for protein sorting at the yeast late Golgi. *Mol. Biol. Cell* **11**, 305-323. doi:10.1091/mbc.11.1.305

Conibear, E., Cleck, J. N. and Stevens, T. H. (2003). Vps51p mediates the association of the GARP (Vps52/53/54) complex with the late Golgi t-SNARE Tlg1p. *Mol. Biol. Cell* **14**, 1610-1623. doi:10.1091/mbc.e02-10-0654

Contractor, A., Rogers, C., Maron, C., Henkemeyer, M., Swanson, G. T. and Heinemann, S. F. (2002). Trans-synaptic Eph receptor-ephrin signaling in hippocampal mossy fiber LTP. *Science* **296**, 1864-1869. doi:10.1126/science.1069081

Deivasigamani, S., Basargekar, A., Shweta, K., Sonavane, P., Ratnaparkhi, G. S. and Ratnaparkhi, A. (2015). A presynaptic regulatory system acts transsynaptically via Mon1 to regulate glutamate receptor levels in drosophila. *Genetics* **201**, 651-664. doi:10.1534/genetics.115.177402

Deshpande, M. and Rodal, A. A. (2016). The crossroads of synaptic growth signaling, membrane traffic and neurological disease: insights from drosophila. *Traffic* **17**, 87-101. doi:10.1111/tra.12345

Dumanchin, C., Czech, C., Campion, D., Cuif, M. H., Poyot, T., Martin, C., Charbonnier, F., Goud, B., Pradier, L. and Frebourg, T. (1999). Presenilins interact with Rab11, a small GTPase involved in the regulation of vesicular transport. *Hum. Mol. Genet.* **8**, 1263-1269. doi:10.1093/hmg/8.7.1263

Falk, J., Konopacki, F. A., Zivraj, K. H. and Holt, C. E. (2014). Rab5 and Rab4 regulate axon elongation in the xenopus visual system. *J. Neurosci.* **34**, 373-391. doi:10.1523/JNEUROSCI.0876-13.2014

Fári, K., Takács, S., Ungár, D. and Sinka, R. (2016). The role of acroblast formation during Drosophila spermatogenesis. *Biol. Open* **5**, 1102-1110. doi:10.1242/bio.018275

Feinstein, M., Flusser, H., Lerman-Sagie, T., Ben-Zeev, B., Lev, D., Agamy, O., Cohen, I., Kadir, R., Sivan, S., Leshinsky-Silver, E. et al. (2014). VPS53 mutations cause progressive cerebello-cerebral atrophy type 2 (PCCA2). *J. Med. Genet.* **51**, 303-308. doi:10.1136/jmedgenet-2013-101823

Folwell, J., Cowan, C. M., Ubhi, K. K., Shiabh, H., Newman, T. A., Shepherd, D. and Mudher, A. (2010). Abeta exacerbates the neuronal dysfunction caused by human tau expression in a Drosophila model of Alzheimer's disease. *Exp. Neurol.* **223**, 401-409. doi:10.1016/j.expneurol.2009.09.014

Greenfield, J. P., Leung, L. W., Cai, D., Kaasik, K., Gross, R. S., Rodriguez-Boulan, E., Greengard, P. and Xu, H. (2002). Estrogen lowers Alzheimer beta-amyloid generation by stimulating trans-Golgi network vesicle biogenesis. *J. Biol. Chem.* **277**, 12128-12136. doi:10.1074/jbc.M110009200

Hirata, T., Fujita, M., Nakamura, S., Gotoh, K., Motooka, D., Murakami, Y., Maeda, Y. and Kinoshita, T. (2015). Post-Golgi anterograde transport requires GARP-dependent endosome-to-TGN retrograde transport. *Mol. Biol. Cell* **26**, 3071-3084. doi:10.1091/mbc.E14-11-1568

Ho, S.-Y., Lorent, K., Pack, M. and Farber, S. A. (2006). Zebrafish fat-free is required for intestinal lipid absorption and Golgi apparatus structure. *Cell Metab.* **3**, 289-300. doi:10.1016/j.cmet.2006.03.001

Jin, E. J., Kiral, F. R., Ozel, M. N., Burchardt, L. S., Osterland, M., Epstein, D., Wolfenberg, H., Prohaska, S.and Hiesinger, P. R. (2018). Live observation of two parallel membrane degradation pathways at axon terminals. *Curr. Biol.* **28**, 1027-1038.e4. doi:10.1016/j.cub.2018.02.032

Karlsson, P., Droce, A., Moser, J. M., Cuhlmann, S., Padilla, C. O., Heimann, P., Bartsch, J. W., Füchtbauer, A., Füchtbauer, E. M. and Schmitt-John, T. (2013). Loss of vps54 function leads to vesicle traffic impairment, protein mis-sorting and embryonic lethality. *Int. J. Mol. Sci.* **14**, 10908-10925. doi:10.3390/ijms140610908

Khodosh, R., Augsburger, A., Schwarz, T. L. and Garrity, P. A. (2006). Bchs, a BEACH domain protein, antagonizes Rab11 in synapse morphogenesis and other developmental events. *Development* **133**, 4655-4665. doi:10.1242/dev.02650

Kittel, R. J., Wichmann, C., Rasse, T. M., Fouquet, W., Schmidt, M., Schmid, A., Wagh, D. A., Pawlu, C., Kellner, R. R., Willig, K. I. et al. (2006). Bruchpilot promotes active zone assembly, Ca2+ channel clustering, and vesicle release. *Science* **312**, 1051-1054. doi:10.1126/science.1126308

Korkut, C. and Budnik, V. (2009). WNTs tune up the neuromuscular junction. *Nat. Rev. Neurosci.* **10**, 627-634. doi:10.1038/nrn2681

Korkut, C., Li, Y., Koles, K., Brewer, C., Ashley, J., Yoshihara, M. and Budnik, V. (2013). Regulation of postsynaptic retrograde signaling by presynaptic exosome release. *Neuron* **77**, 1039-1046. doi:10.1016/j.neuron.2013.01.013

Lahey, T., Gorczyca, M., Jia, X.-X. and Budnik, V. (1994). The Drosophila tumor suppressor gene dlg is required for normal synaptic bouton structure. *Neuron* **13**, 823-835. doi:10.1016/0896-6273(94)90249-6

Lasiecka, Z. M. and Winckler, B. (2011). Mechanisms of polarized membrane trafficking in neurons – focusing in on endosomes. *Mol. Cell. Neurosci.* **48**, 278-287. doi:10.1016/j.mcn.2011.06.013

Li, X., Sapp, E., Chase, K., Comer-Tierney, L. A., Masso, N., Alexander, J., Reeves, P., Kegel, K. B., Valencia, A., Esteves, M. et al. (2009a). Disruption of Rab11 activity in a knock-in mouse model of Huntington's disease. *Neurobiol. Dis.* **36**, 374-383. doi:10.1016/j.nbd.2009.08.003

Li, X., Standley, C., Sapp, E., Valencia, A., Qin, Z. H., Kegel, K. B., Yoder, J., Comer-Tierney, L. A., Esteves, M., Chase, K. et al. (2009b). Mutant huntingtin impairs vesicle formation from recycling endosomes by interfering with Rab11 activity. *Mol. Cell. Biol.* **29**, 6106-6116. doi:10.1128/MCB.00420-09

Li, X., Valencia, A., Sapp, E., Masso, N., Alexander, J., Reeves, P., Kegel, K. B., Aronin, N. and Difiglia, M. (2010). Aberrant Rab11-dependent trafficking of the neuronal glutamate transporter EAAC1 causes oxidative stress and cell death in Huntington's disease. *J. Neurosci.* **30**, 4552-4561. doi:10.1523/JNEUROSCI.5865-09.2010

Li, J., Kanekiyo, T., Shinohara, M., Zhang, Y., LaDu, M. J., Xu, H. and Bu, G. (2012). Differential regulation of amyloid-beta endocytic trafficking and lysosomal degradation by apolipoprotein E isoforms. *J. Biol. Chem.* **287**, 44593-44601. doi:10.1074/jbc.M112.420224

Livak, K. J. and Schmittgen, T. D. (2001). Analysis of relative gene expression data using real-time quantitative PCR and the 2(−Delta Delta C(T)) method. *Methods* **25**, 402-408. doi:10.1006/meth.2001.1262

Menon, K. P., Carrillo, R. A. and Zinn, K. (2013). Development and plasticity of the Drosophila larval neuromuscular junction. *Wiley Interdiscip. Rev. Dev. Biol.* **2**, 647-670. doi:10.1002/wdev.108

Moser, J. M., Bigini, P. and Schmitt-John, T. (2013). The wobbler mouse, an ALS animal model. *Mol. Genet. Genomics* **288**, 207-229. doi:10.1007/s00438-013-0741-0

Mudher, A., Shepherd, D., Newman, T. A., Mildren, P., Jukes, J. P., Squire, A., Mears, A., Drummond, J. A., Berg, S., MacKay, D. et al. (2004). GSK-3beta inhibition reverses axonal transport defects and behavioural phenotypes in Drosophila. *Mol. Psychiatry* **9**, 522-530. doi:10.1038/sj.mp.4001483

Nesler, K. R., Starke, E. L., Boin, N. G., Ritz, M. and Barbee, S. A. (2016). Presynaptic CamKII regulates activity-dependent axon terminal growth. *Mol. Cell. Neurosci.* **76**, 33-41. doi:10.1016/j.mcn.2016.08.007

Nijhof, B., Castells-Nobau, A., Wolf, L., Scheffer-de Gooyert, J. M., Monedero, I., Torroja, L., Coromina, L., van der Laak, J. A. W. M. and Schenck, A. (2016). A new Fiji-based algorithm that systematically quantifies nine synaptic parameters provides insights into Drosophila NMJ morphometry. *PLoS Comput. Biol.* **12**, e1004823. doi:10.1371/journal.pcbi.1004823

Palmisano, R., Golfi, P., Heimann, P., Shaw, C., Troakes, C., Schmitt-John, T. and Bartsch, J. W. (2011). Endosomal accumulation of APP in wobbler motor neurons reflects impaired vesicle trafficking: implications for human motor neuron disease. *BMC Neurosci.* **12**, 24. doi:10.1186/1471-2202-12-24

Parnas, D., Haghighi, A. P., Fetter, R. D., Kim, S. W. and Goodman, C. S. (2001). Regulation of postsynaptic structure and protein localization by the Rho-type guanine nucleotide exchange factor dPix. *Neuron* **32**, 415-424. doi:10.1016/S0896-6273(01)00485-8

Pérez-Victoria, F. J. and Bonifacino, J. S. (2009). Dual roles of the mammalian GARP complex in tethering and SNARE complex assembly at the trans-Golgi network. *Mol. Cell. Biol.* **29**, 5251-5263. doi:10.1128/MCB.00495-09

Pérez-Victoria, F. J., Mardones, G. A. and Bonifacino, J. S. (2008). Requirement of the human GARP complex for mannose 6-phosphate-receptor-dependent sorting of cathepsin D to lysosomes. *Mol. Biol. Cell* **19**, 2350-2362. doi:10.1091/mbc.e07-11-1189

Pfeffer, S. R. (2017). Rab GTPases: master regulators that establish the secretory and endocytic pathways. *Mol. Biol. Cell* **28**, 712-715. doi:10.1091/mbc.e16-10-0737

Pfeffer, S. and Aivazian, D. (2004). Targeting RAB GTPases to distinct membrane compartments. *Nat. Rev. Mol. Cell Biol.* **5**, 886-896. doi:10.1038/nrm1500

Ponomareva, O. Y., Eliceiri, K. W. and Halloran, M. C. (2016). Charcot-Marie-Tooth 2b associated Rab7 mutations cause axon growth and guidance defects during vertebrate sensory neuron development. *Neural Dev.* **11**, 2. doi:10.1186/s13064-016-0058-x

Poteryaev, D., Fares, H., Bowerman, B. and Spang, A. (2007). Caenorhabditis elegans SAND-1 is essential for RAB-7 function in endosomal traffic. *EMBO J.* **26**, 301-312. doi:10.1038/sj.emboj.7601498

Pradhan, S. J., Nesler, K. R., Rosen, S. F., Kato, Y., Nakamura, A., Ramaswami, M. and Barbee, S. A. (2012). The conserved P body component HPat/Pat1 negatively regulates synaptic terminal growth at the larval Drosophila neuromuscular junction. *J. Cell Sci.* **125**, 6105-6116. doi:10.1242/jcs.113043

Quenneville, N. R., Chao, T. Y., McCaffery, J. M. and Conibear, E. (2006). Domains within the GARP subunit Vps54 confer separate functions in complex assembly and early endosome recognition. *Mol. Biol. Cell* **17**, 1859-1870. doi:10.1091/mbc.e05-11-1002

Ramos, C. I., Igiesuorobo, O., Wang, Q. and Serpe, M. (2015). Neto-mediated intracellular interactions shape postsynaptic composition at the Drosophila neuromuscular junction. *PLoS Genet.* **11**, e1005191. doi:10.1371/journal.pgen.1005191

Richards, P., Didszun, C., Campesan, S., Simpson, A., Horley, B., Young, K. W., Glynn, P., Cain, K., Kyriacou, C. P., Giorgini, F., Nicotera, P. et al. (2011). Dendritic spine loss and neurodegeneration is rescued by Rab11 in models of Huntington's disease. *Cell Death Differ.* **18**, 191-200. doi:10.1038/cdd.2010.127

Riedel, F., Gillingham, A. K., Rosa-Ferreira, C., Galindo, A. and Munro, S. (2016). An antibody toolkit for the study of membrane traffic in Drosophila melanogaster. *Biol. Open* **5**, 987-992. doi:10.1242/bio.018937

Sakuma, C., Kawauchi, T., Haraguchi, S., Shikanai, M., Yamaguchi, Y., Gelfand, V. I., Luo, L. Q., Miura, M. and Chihara, T. (2014). Drosophila Strip serves as a platform for early endosome organization during axon elongation. *Nat. Commun.* **5**, 5180. doi:10.1038/ncomms6180

Satoh, D., Sato, D., Tsuyama, T., Saito, M., Ohkura, H., Rolls, M. M., Ishikawa, F. and Uemura, T. (2008). Spatial control of branching within dendritic arbors by dynein-dependent transport of Rab5-endosomes. *Nat. Cell Biol.* **10**, 1164-1171. doi:10.1038/ncb1776

Schindelin, J., Arganda-Carreras, I., Frise, E., Kaynig, V., Longair, M., Pietzsch, T., Preibisch, S., Rueden, C., Saalfeld, S., Schmid, B. J. Y. et al. (2012). Fiji: an open-source platform for biological-image analysis. *Nat. Methods* **9**, 676-682. doi:10.1038/nmeth.2019

Schindelin, J., Rueden, C. T., Hiner, M. C. and Eliceiri, K. W. (2015). The ImageJ ecosystem: an open platform for biomedical image analysis. *Mol. Reprod. Dev.* **82**, 518-529. doi:10.1002/mrd.22489

Schindler, C., Chen, Y., Pu, J., Guo, X. and Bonifacino, J. S. (2015). EARP is a multisubunit tethering complex involved in endocytic recycling. *Nat. Cell Biol.* **17**, 639-650. doi:10.1038/ncb3129

Schmitt-John, T. (2015). VPS54 and the wobbler mouse. *Front. Neurosci.* **9**, 381. doi:10.3389/fnins.2015.00381

Schmitt-John, T., Drepper, C., Mußmann, A., Hahn, P., Kuhlmann, M., Thiel, C., Hafner, M., Lengeling, A., Heimann, P., Jones, J. M. et al. (2005). Mutation of Vps54 causes motor neuron disease and defective spermiogenesis in the wobbler mouse. *Nat. Genet.* **37**, 1213-1215. doi:10.1038/ng1661

Schreij, A. M. A., Fon, E. A. and McPherson, P. S. (2016). Endocytic membrane trafficking and neurodegenerative disease. *Cell. Mol. Life Sci.* **73**, 1529-1545. doi:10.1007/s00018-015-2105-x

Shahidullah, M., Le Marchand, S. J., Fei, H., Zhang, J., Pandey, U. B., Dalva, M. B., Pasinelli, P. and Levitan, I. B. (2013). Defects in synapse structure and function precede motor neuron degeneration in Drosophila models of FUS-related ALS. *J. Neurosci.* **33**, 19590-19598. doi:10.1523/JNEUROSCI.3396-13.2013

Siniossoglou, S. and Pelham, H. R. B. (2002). Vps51p links the VFT complex to the SNARE Tlg1p. *J. Biol. Chem.* **277**, 48318-48324. doi:10.1074/jbc.M209428200

Sisson, J. C., Field, C., Ventura, R., Royou, A. and Sullivan, W. (2000). Lava lamp, a novel peripheral Golgi protein, is required for Drosophila melanogaster cellularization. *J. Cell Biol.* **151**, 905-918. doi:10.1083/jcb.151.4.905

Steinert, J. R., Campesan, S., Richards, P., Kyriacou, C. P., Forsythe, I. D. and Giorgini, F. (2012). Rab11 rescues synaptic dysfunction and behavioural deficits in a Drosophila model of Huntington's disease. *Hum. Mol. Genet.* **21**, 2912-2922. doi:10.1093/hmg/dds117

Sulkowski, M. J., Han, T. H., Ott, C., Wang, Q., Verheyen, E. M., Lippincott-Schwartz, J. and Serpe, M. (2016). A novel, noncanonical BMP pathway modulates synapse maturation at the Drosophila neuromuscular junction. *PLoS Genet.* **12**, e1005810. doi:10.1371/journal.pgen.1005810

Tanaka, T. and Nakamura, A. (2008). The endocytic pathway acts downstream of Oskar in Drosophila germ plasm assembly. *Development* **135**, 1107-1117. doi:10.1242/dev.017293

Tinevez, J.-Y., Perry, N., Schindelin, J., Hoopes, G. M., Reynolds, G. D., Laplantine, E., Bednarek, S. Y., Shorte, S. L. and Eliceiri, K. W. (2017). TrackMate: an open and extensible platform for single-particle tracking. *Methods* **115**, 80-90. doi:10.1016/j.ymeth.2016.09.016

van Bergeijk, P., Adrian, M., Hoogenraad, C. C. and Kapitein, L. C. (2015). Optogenetic control of organelle transport and positioning. *Nature* **518**, 111-114. doi:10.1038/nature14128

Wagh, D. A., Rasse, T. M., Asan, E., Hofbauer, A., Schwenkert, I., Dürrbeck, H., Buchner, S., Dabauvalle, M.-C., Schmidt, M., Qin, G. et al. (2006). Bruchpilot, a protein with homology to ELKS/CAST, is required for structural integrity and function of synaptic active zones in Drosophila. *Neuron* **51**, 275. doi:10.1016/j.neuron.2006.06.022

West, R. J., Lu, Y., Marie, B., Gao, F. B. and Sweeney, S. T. (2015). Rab8, POSH, and TAK1 regulate synaptic growth in a Drosophila model of frontotemporal dementia. *J. Cell Biol.* **208**, 931-947. doi:10.1083/jcb.201404066

Wojnacki, J. and Galli, T. (2016). Membrane traffic during axon development. *Dev. Neurobiol.* **76**, 1185-1200. doi:10.1002/dneu.22390

Yousefian, J., Troost, T., Grawe, F., Sasamura, T., Fortini, M. and Klein, T. (2013). Dmon1 controls recruitment of Rab7 to maturing endosomes in Drosophila. *J. Cell Sci.* **126**, 1583-1594. doi:10.1242/jcs.114934

Zhang, J., Schulze, K. L., Hiesinger, P. R., Suyama, K., Wang, S., Fish, M., Acar, M., Hoskins, R. A., Bellen, H. J. and Scott, M. P. (2007). Thirty-one flavors of Drosophila rab proteins. *Genetics* **176**, 1307-1322. doi:10.1534/genetics.106.066761

Zhu, J.-Y., Vereshchagina, N., Sreekumar, V., Burbulla, L. F., Costa, A. C., Daub, K. J., Woitalla, D., Martins, L. M., Krüger, R. and Rasse, T. M. (2013). Knockdown of Hsc70-5/mortalin induces loss of synaptic mitochondria in a Drosophila Parkinson's disease model. *Plos ONE* **8**, e83714. doi:10.1371/journal.pone.0083714

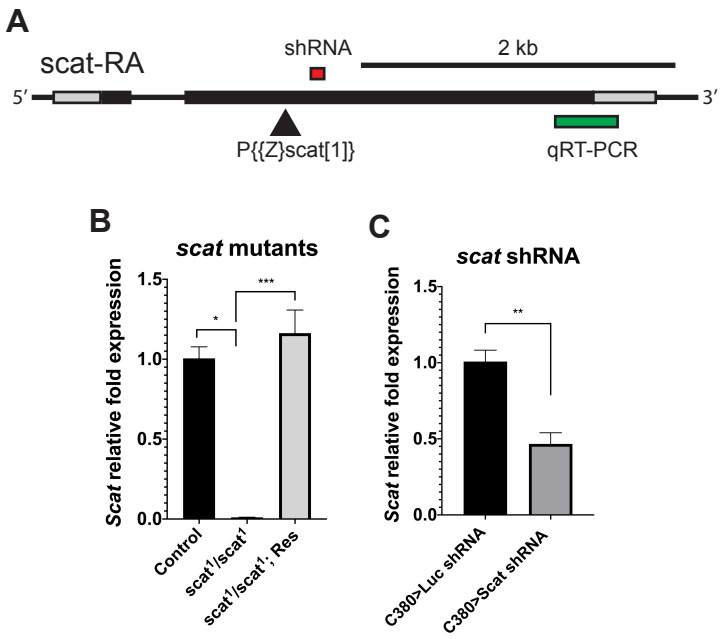

Fig. S1. The *scat*^{1} allele. (A) This is a diagram showing the structure of the *scat* gene in *Drosophila*. Exons are indicated by boxes and the single intron indicated by a line. Gray boxes at the 3' and 5' ends indicate the untranslated regions (UTRs) and black boxes indicate coding sequence. The triangle shows the location of the P-element insertion in the second exon of the *scat* locus. Using an antibody targeting the N-terminal 200 amino acids of the Scat protein, it has previously been shown that this is a null allele (Fari et al., 2016). The region targeted by the *UAS-TRiP(HMS01910)* shRNA line is indicated by the red box. The green box at the 3' end indicates the location of the amplicon analyzed for qRT-PCR. (B) Results of qRT-PCR analysis of *scat* mRNA levels in the larval CNS of controls, *scat*^{1} homozygotes, and the *scat*^{1}*/scat*^{1}*; scat-HA:scat/scat-HA:scat* rescue (Res) lines. *scat* mRNA is reduced in *scat*^{1} homozygotes and restored to near control levels in the rescue line. (C) Results of qRT-PCR analysis of *scat* mRNA levels in control (*C380>Luc shRNA*) and *scat* (*C380>scat shRNA*) larval ventral ganglia. Levels of *scat* mRNA are reduced by at least 50%. Note that this is likely an underrepresentation because *C380-Gal4* drives expression in only a subset of neurons in the ventral ganglion. In both B and C, levels of *scat* transcripts were determined as described in the Methods and then normalized to the control. *N* = 7 ventral ganglia for each genotype. qPCR data shown in B was analyzed by one-way ANOVA followed by a Holm-Sidak multiple comparison test. qPCR data shown in C was analyzed by a two-way Student's t-test. Data are represented as the mean ± SEM for three technical replicates. * $p < 0.05$, ** $p < 0.01$, *** $p < 0.001$.

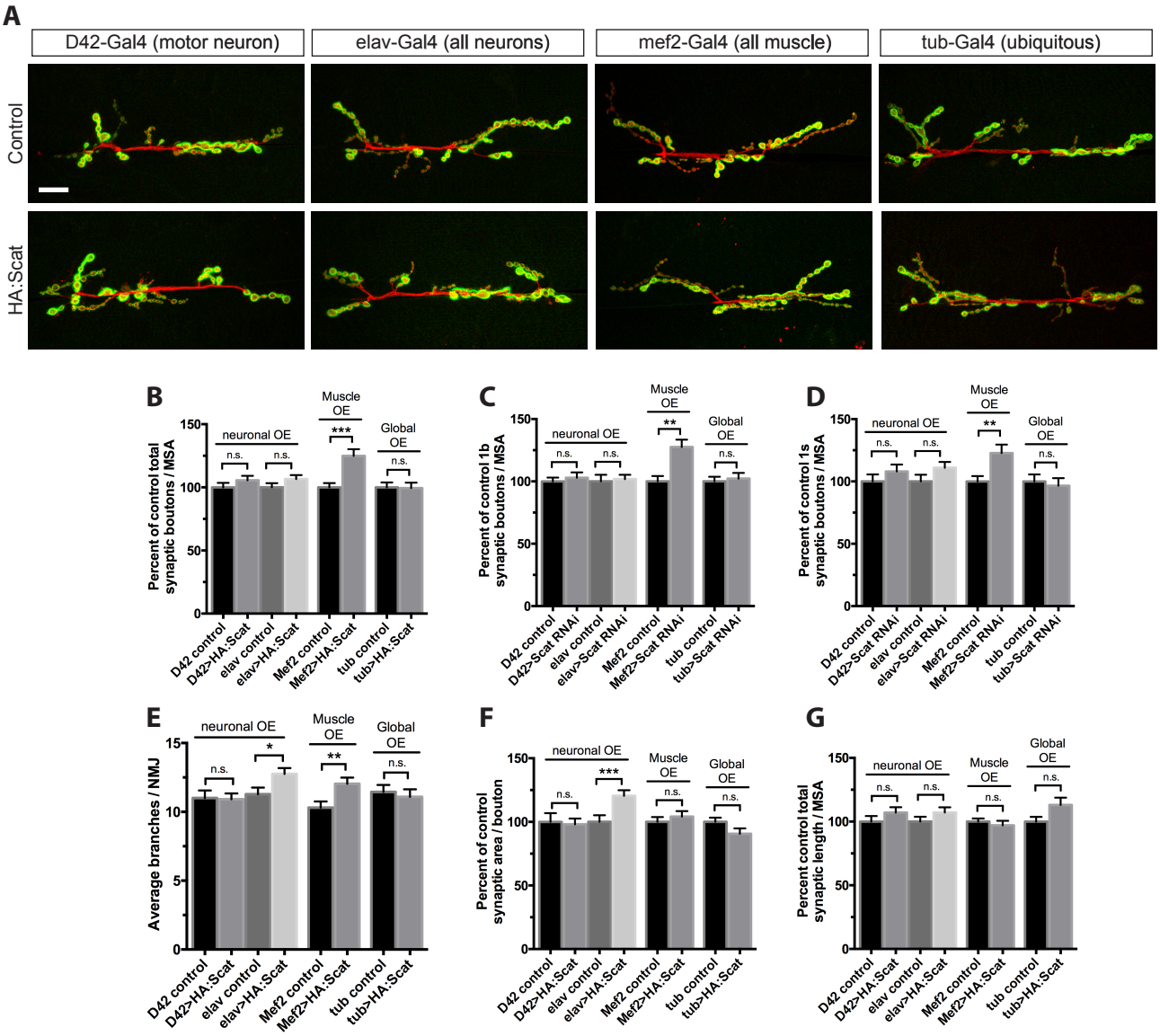

Fig. S2. Overexpression of *scat* has an effect on NMJ development. (A) The inducible *UAS-HA:scat* transgene was expressed using a motor neuron-specific driver (*D42-Gal4*), a strong pan-neuronal driver (*elav-Gal4*), a strong muscle-specific driver (*Mef2-Gal4*), or ubiquitously (*tubulin-Gal4*). NMJs at m6/7 in body segment A3 have been stained with antibodies targeting Dlg (green) and HRP (red). Images show maximum Z-projections. Scale bar, 20 μm. Quantification of the (B) total number of boutons, (C) type 1b boutons, and (D) type 1s boutons shows that bouton number is increased when HA:Scat is overexpressed in larval muscle but not when expressed ubiquitously or in neurons. (E) The number of branches is significantly increased when HA:Scat is strongly expressed in either neurons or muscle. For B-E, $N = 22, 23, 19, 24, 30, 30, 23$, and 23 in the order shown in graphs. (F) Total synaptic area is increased when strongly expressed in muscle. (G)

There is no impact on total synaptic length. Synaptic area and length where quantified using the Morphometrics algorithm. For F and G, *N* = 22, 23, 19, 24, 28, 30, 24, and 27 in the order shown in graphs. All statistical analysis was done by Kruskal-Wallis followed by a Dunn's multiple comparison test. Unless otherwise indicated, all statistical comparisons shown have been compared to driver-specific controls (*driver*/+ heterozygotes). * $p < 0.05$, ** $p < 0.01$, *** $p < 0.001$.

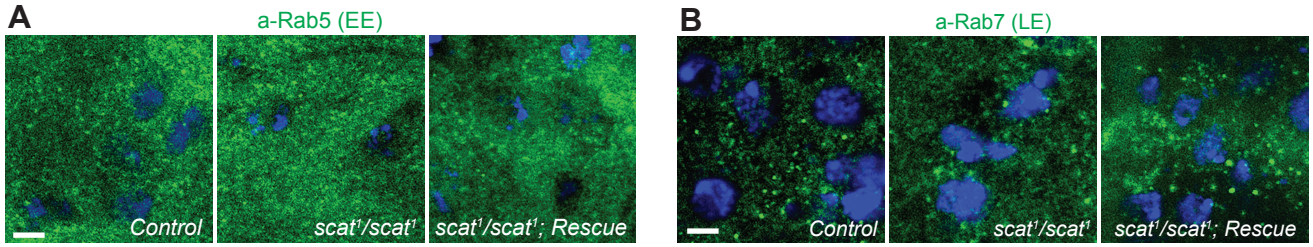

Fig. S3. *scat* mutants do not have defects in Rab5- or Rab7-positive endosomes. Using polyclonal antibodies targeting Rab5 and Rab7 (Hirata et al., 2015), there is no visible defect in the size, number, or distribution of EE or LE in *scat*^{1} mutant MNs. Images shown are single focal planes. Ventral ganglia from wandering third instar larvae from controls, *scat*^{1} homozygotes, and the *scat*^{1}*/scat*^{1}*; scat-HA:scat/scat-HA:scat* rescue lines were stained with antibodies targeting (A) Rab5 or (B) Rab7 (both green). Nuclei are marked by DAPI (blue). Scale bar, 2.5 μm.

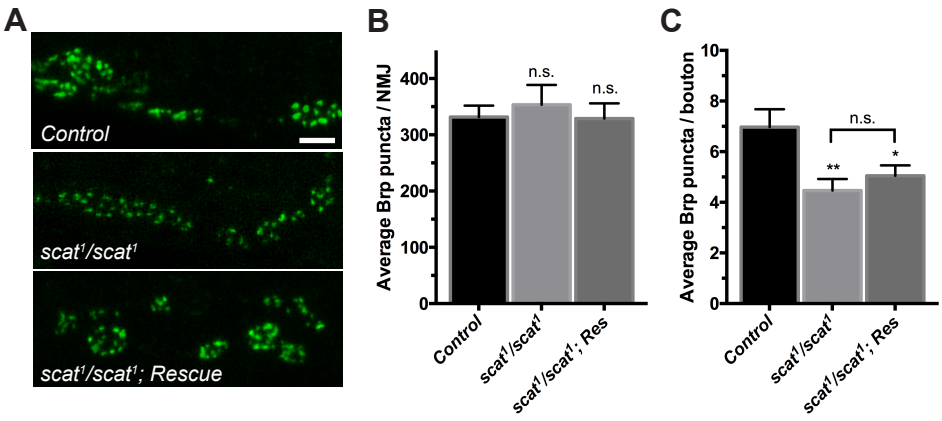

Fig. S4. *scat* mutants do not have active zone defects. A) NMJs innervating muscle 6/7 in body segment A3 from the indicated genotypes stained with an antibody targeting Brp (green). *scat* mutants have an increased number of small boutons with fewer Brp-positive puncta. Scale bar, 5 μm. B) The total number of Brp-positive punctae per NMJ does not change C) The number of Brp-positive punctae per synaptic bouton increases in *scat* mutants. $N = 10$ for each genotype. Statistical analysis was done using a one-way ANOVA followed by a Holm-Sidak multiple comparison test. Data in graphs are represented by the mean ± SEM.

Table S1.

Primer list:

Cloning of *scat* from LD2244 into pUAST (to generate the inducible HA:Scat line)	
Primer pair	Sequence (5' to 3')
Scat_HAf	GATCTTGCGGCCGCATGGCC ACGACAAGATCCGC
Scat_HAr	GGTACCCTCGAGTTAAGCGTAATCTGGAACATCGTA TGGGTAGTAGAGCCAGATCTCCTCCA
Cloning of *scat* from genomic DNA into pCASPR (to generate the genomic rescue line)	
Primer pair	Sequence (5' to 3')
Scat rescue F1	GATCTTGCGGCCGCGTCAGCTGATTTTGCTCAGA
Scat rescue R1	TCAAGCGTAATCTGGAACATCGTATGGGTAGTAGAGCCAGATCTCCTCCA
Scat rescue F2	TACCCATACGATGTTCCAGATTACGCTTGAGCATTCCGAAGTATTCCATA
Scat rescue R2	GGTACCCTCGAGCTTTCACCCCTAAGTTGCAT
Quantitative RT-PCR experiments (for Fig. S1)	
Primer pair	Sequence (5' to 3')
Scat_qPf	ACGAAACTATCGAGCGGGAC
Scat_qPr	TTGAGCTGCCAATCTCTCGG
RpS3_qPf	TCTTTCTTTTCTGCGCACCA
RpS3_qPr	TCGCATTCATTTTGACGTCG